

UNCLASSIFIED

AD 295835

*Reproduced
by the*

**ARMED SERVICES TECHNICAL INFORMATION AGENCY
ARLINGTON HALL STATION
ARLINGTON 12, VIRGINIA**



UNCLASSIFIED

NOTICE: When government or other drawings, specifications or other data are used for any purpose other than in connection with a definitely related government procurement operation, the U. S. Government thereby incurs no responsibility, nor any obligation whatsoever; and the fact that the Government may have formulated, furnished, or in any way supplied the said drawings, specifications, or other data is not to be regarded by implication or otherwise as in any manner licensing the holder or any other person or corporation, or conveying any rights or permission to manufacture, use or sell any patented invention that may in any way be related thereto.

AD 295835
RADC-TDR-62-496, VOL. I

1 AUGUST 1962

Study of Interference Aspects of Fresnel Region Phenomena

VOLUME I

MATHEMATICAL DEVELOPMENT OF NEAR FIELD THEORY

R. A. Gerlock

AMERICAN SYSTEMS Incorporated
Systems Division
Hawthorne, California

ASI TECHNICAL REPORT NO. 62-ESD-14
FINAL REPORT
CONTRACT NO. AF30(602)-2507

Prepared for

ROME AIR DEVELOPMENT CENTER
AIR FORCE SYSTEMS COMMAND
UNITED STATES AIR FORCE
GRIFFISS AIR FORCE BASE, NEW YORK

295835

1. When Government drawings, specifications, or other data are used for any purpose other than in connection with a definitely related Government procurement operation, the United States Government thereby incurs no responsibility nor any obligation whatsoever and the fact that the Government may have formulated, furnished, or in any way supplied the said drawings, specifications, or other data is not to be regarded by implication or otherwise as in any manner licensing the holder or any other person or corporation, or conveying any rights or permission to manufacture, use, or sell any patented invention that may in any way be related thereto.

2. Qualified requestors may obtain copies of this report from the ASTIA Document Service Center, Dayton 2, Ohio. ASTIA services for the Department of Defense contractors are available through the "Field of Interest Register" on a "need-to-know" certified by the cognizant military agency of this project or contract.

STUDY OF INTERFERENCE ASPECTS
OF FRESNEL REGION PHENOMENA

VOLUME I

Mathematical Development of Near Field Theory

R. A. Gerlock
AMERICAN SYSTEMS Incorporated
Electromagnetic Systems Division
Hawthorne, California

ASI Technical Report No. 62-ESD-14
Final Report

Contract No. AF30(602)-2507
Project No. 4540
Task No. 45169

Prepared for

Rome Air Development Center
Air Force Systems Command
United States Air Force
Griffiss Air Force Base, New York

FOREWARD

This volume is the first of two, comprising the final report on Contract AF30(602)-2507. Volume I is primarily limited to an explanation and justification of the theoretical approaches used in the study of the Interference Aspects of Fresnel Region Phenomena. Volume II presents the most important results of this study and describes the manner in which these results can be used to determine the near field characteristics of high gain antennas.

Suggestions of Mr. H. E. Shanks were instrumental to the successful completion of several phases of the work, and are gratefully acknowledged. The assistance of Messrs. M. V. Lopez, G. E. Martes, and R. K. McFadden in the theoretical and experimental portions of the study were also of significant value. Messrs. J. J. Hilton and E. E. Stafford ably performed the computer programming and the associated computations.

ABSTRACT

The spatial distribution of energy associated with typical antennas has been investigated in the region of the forward hemisphere which is relatively close to the antennas. This region is referred to as the scalar near field region (SNF), and it extends inward to about one antenna diameter from the aperture plane, and outward to the far field region. In the SNF region the radial components of field are negligible, and the fields may be obtained by a scalar formulation; however, the standard Fresnel or Fraunhofer approximations are not valid throughout this region.

The study has resulted in a tabulated set of field components from which the value of the SNF of in-phase circular and rectangular apertures can readily be calculated. The apertures' sizes and distribution functions can be selected arbitrarily. Thus, the results are applicable to a variety of antennas existing in the field.

The Fresnel-Fraunhofer transition distance has been determined as a function of azimuth angle, for various aperture distributions. The transition distance decreases rapidly as the azimuthal angle increases. At small angles the transition distance increases as the antenna's sidelobe level is lowered and as its sidelobe taper is decreased. The maximum transition distance varies between somewhat less than L^2/λ and $5L^2/\lambda$ depending upon the antenna's sidelobe level and taper. (L is the antenna length and λ is the wavelength.) At azimuthal angles which are large compared with an antenna beamwidth, the effect of the sidelobe level and taper diminishes, and the transition distance approaches $L/\sin \theta$ where θ is the angle from broadside.

CONTENTS

	Page
Foreward	ii
Abstract	iii
I. INTRODUCTION	1
II. APPROACH AND SUMMARY	3
III. ANALYSIS OF WORK PROGRESS	8
A. Discussion of Antenna Fields	8
B. Scalar Near Field to Far Field Transition Region . . .	14
C. SNF of Circular Apertures	35
1. Mathematical Formulation	35
2. Computer Program	38
3. Evaluation of the SNF	40
4. Universal SNF Patterns	44
5. Accuracy of the Scalar Near Field Formulation . .	51
6. On-Axis Field	51
D. Rectangular Apertures	54
1. Approach	54
2. Angular Variations of the SNF	55
3. Range Variations of the SNF	60
4. Mathematical Formulation	63
5. Evaluation of the SNF	63

CONTENTS (Continued)

	Page
E. E. Additional Considerations	64
F. Pattern Measurement	71
G. Experimental Program	73
1. Test Apparatus	73
2. Parabolic Reflector	77
3. Linear Array.	81
4. Circular Planar Array	85
IV. CONCLUSIONS.	89
V. RECOMMENDATIONS FOR FUTURE RESEARCH.	91
APPENDICES	
I. Asymptotic Representation of the Transition Distance	94
II. Program for the Evaluation of $J_v(x)$	97
References	99
General Bibliography	101

ILLUSTRATIONS

		Page
1.	Coordinate Frame	9
2.	Calculated Field of Nine-Element Tchebyscheff Array . . .	16
3.	Transition Distance — 4.5 db Sidelobe Taper	24
4.	Transition Distance — 7.6 db Sidelobe Taper	26
5.	Transition Distance — 0 db Sidelobe Taper	27
6.	Variation in First Null Transition Distances	28
7.	Fresnel Field Strength in Direction of Far Field Zeros and at the Transition Distance — Uniform Distribution . .	32
8.	Aperture Distribution Parameters Versus Aperture Taper for High-Gain Paraboloidal Type Reflectors	42
9.	Comparison of the SNF of 10λ and 160λ Apertures at Approximate Range of $R = 0.12 D^2/\lambda$ — Uniform Distribution.	46
10.	Comparison of the SNF of 10λ and 160λ Apertures at Approximate Range of $R = 0.12 D^2/\lambda$ — $(1 - \rho^2)$ Distribution.	47
11.	Comparison of the SNF of 80λ and 160λ Apertures at Approximate Range of $R = 0.015 D^2/\lambda$ — Uniform Distribution.	48
12.	Comparison of the SNF of 80λ and 160λ Apertures at Approximate Range of $R = 0.015 D^2/\lambda$ — $(1 - \rho^2)$ Distribution.	49
13.	Comparison of Scalar Near Field Theory with Exact Theory	52
14.	Maximum Phase Error in Rectangular Aperture Versus Range.	62

ILLUSTRATIONS (Continued)

	Page
15. Single-Surface Lens for Antenna Focusing	74
16. On-Axis Field Measuring Setup.	75
17. On-Axis Power Measurement - Sample Data	78
18. Four-Foot X-Band Parabolic Dish.	79
19. Aperture Field of Four-Foot Parabolic Dish	80
20. On-Axis Field of Four-Foot Paraboloid Reflector, -40λ Diameter at X-Band	82
21. Forty-Element Linear Array	83
22. On-Axis Power — Uniformly Illuminated Line Source, $L = 27.3 \lambda$	84
23. Circular Planar Array of Five Rings of Crossed Slots — Side View	86
24. Circular Planar Array of Five Rings of Crossed Slots — Front View	87
25. On-Axis Field for Circular Planar Array — Diameter is 10.73λ	88
26. Division of $v-x$ Plane	98

I. INTRODUCTION

The increasing complexity and intermingling of radars, communications equipment, and other electronic gear, has led to considerable concern over the mutual RF interference problems present in high-density site environments. Of considerable importance, in terms of lowering the interference levels, is proper equipment location and site configuration. A sound engineering approach to this problem must be based on reliable field strength data in the site environment. The purpose of the present program is to provide engineering data and design analysis techniques for the radiated field strengths in regions relatively close to typical antenna structures.

Significant contributions to the study of Fresnel and near zone radiation phenomena have been made by a number of organizations, too numerous for individual mention. The more notable efforts in this area are listed in the General Bibliography included in this volume. However, past investigations have not been of sufficient scope to provide definitive results for the purposes of RFI prediction. Thus, one of the principal aims of the present program has been to develop simple techniques by which field and laboratory personnel can readily determine the near fields of arbitrarily-excited antennas.

The study program had several specific objectives; each related to the interference properties of the "near" field. As mentioned previously, the primary objective was to theoretically determine the spatial distribution of energy associated with typical antennas. A second important objective was to determine the Fresnel-Fraunhofer transition distance, which is the distance at which the far field approximations can be used to accurately predict the signal density. Additionally, the effects of operating at nondesign

frequencies and of terrain reflections were touched upon. Also, a study of focusing techniques to allow far field pattern measurement in the near field was initiated. Finally, the theoretical techniques were verified by experimental measurements of the on-axis power densities for typical radiating apertures.

This volume is the first of a two volume final report. It is primarily limited to an adequate description of the theoretical approaches used in the program, a justification of the approximations used, and the experimental verification of the results. The second volume is intended to be used as a handbook for estimating the near field characteristics of typical antennas. To a large extent, the second volume is comprised of two tables, from which the near-zone signal strengths of circular and rectangular apertures can be calculated.

The following section discusses in general terms the approach to the problem and a summary of the results.

II. APPROACH AND SUMMARY

The first step towards a solution to the near field problem was to establish a suitable mathematical formulation for the radiated fields. The common practice of reducing the vector problem to a scalar problem by making suitable approximations to the exact solution was followed. This step effectively restricts the solutions to the region of space that is exterior to a sphere which just encloses the antenna of interest. It is felt that this restriction is not severe in view of the fact that electronic equipments are seldom located within an antenna diameter of each other.

Because of the scalar formulation, the region in which the solutions for the radiated fields are valid is referred to as the scalar near field (SNF). For convenience, it is defined as extending inward to about one antenna diameter from the aperture plane and outward to the far field region. A more complete description of the approximations made in the basic mathematical formulation, as well as a general discussion of antenna field regions, is presented in Section III. A.

As indicated previously, one of the principal aims of the study program was to develop techniques which allow field and laboratory personnel to determine the near fields of arbitrarily-excited antennas by fairly simple methods. To be of widespread value, these techniques must not require the use of special equipment such as electronic computers, and should yield the SNF by methods which are about as simple as those used to determine far field patterns. Achievement of these ends was complicated by a number of factors:

(a) While the near and far zone diffraction fields are both obtained by integrating currents over the radiating aperture, the integrals are, without exception, much more difficult to evaluate in the near zone than in the far zone. This has necessitated the use of high-speed electronic computers in the near zone investigations.

(b) The far field pattern shape is independent of range, while the near field pattern shape is not; thus, a family of curves is required to describe an antenna's near field, while a single curve suffices to describe its far field.

(c) The far field patterns of antennas which are identical except for size, are identical except for an angular scale factor. However, the near field patterns of such antennas are not simply related. This implies it is necessary to perform an independent analysis each time the antenna size is varied.

To overcome the above difficulties, without severely restricting either the accuracy or the general utility of the results, several techniques for reducing the required number of data points were discovered and incorporated in the present program.

The first technique concerned the types of aperture distributions investigated. For the case of circular apertures, the distribution functions chosen for study were selected to be of the form $1 + a_1 \rho^2 + a_2 \rho^4 + a_3 \rho^6$, where ρ is the normalized radius and the a 's are parameters which control the shape of the aperture distribution. By varying the values of a , this class of functions can be made to closely approximate a wide range of distributions which occur in practice. The total near field is given by

the sum of the field components arising from each of the four terms in the aperture distribution. The values of a effect only the magnitudes of the field components; thus, by calculating the components with each a equated to unity, a fundamental set of field components is obtained. The SNF of an arbitrarily-excited antenna can be calculated from this set by adjusting the magnitude of the individual components by the appropriate values of a , and summing. This approach eliminates the need for treating a large number of aperture distributions and insures that the results of the study program will be applicable to most cases arising in practice. An almost identical approach was used for the rectangular aperture case.

The number of required data points was further reduced by determining the conditions under which the signal densities can be accurately calculated by use of the far field expressions. It was discovered that the wide angle fields can be accurately predicted by use of the far field expressions at distances very much less than the commonly accepted far field distance given by $2D^2/\lambda$.

The analysis from which the transition distance was determined was based on a criterion which limits the near field strength, in directions in which the far field vanishes. This insures that, at distances equal to or greater than the transition distance, the values of the SNF does not significantly differ from the far field value. A number of different types of aperture distributions were studied in this connection. It has been demonstrated that the transition distance depends primarily upon the antenna's sidelobe level, the sidelobe taper, and the azimuthal angle to the field point. In general, as the sidelobe level decreases, the transition distance increases. As the azimuthal angle increases, the transition distance decreases and becomes less dependent on the antenna's sidelobe level and taper. It was

determined that at sufficiently wide angles, the transition distance goes approximately as $\frac{D}{\sin \theta}$, and the SNF tends towards the envelope of the far field pattern.

Use of the far field data at distances greater than the transition distance greatly reduces the volume in space in which the scalar near field must be determined, and reduces the number of data points which must be obtained. In the present program, a 50 percent reduction in the required number of data points was affected by incorporating this feature.

The greatest saving in the required number of data points was affected by eliminating the need for independent analyses each time the antenna size is varied. This was the result of an analysis which established the conditions that permit the prediction of the SNF of an antenna from that of a similar antenna of different size. It was determined that if the near fields are compared in u-space (where $u = \frac{\pi D}{\lambda} \sin \theta$) and at carefully chosen values of range (approximately given by constant values of $R\lambda/D^2$), the differences are insignificant for ratios of antenna sizes as great as sixteen-to-one.

In the study program, a number of comparisons were made in order to definitely establish the fact that universal patterns for the SNF can be constructed. Uniform and $1 - \rho^2$ distributions were considered. The largest ratio of antenna sizes considered was 16:1 (10λ and 160λ diameter apertures), and the smallest value of range corresponded to only $0.0150 D^2/\lambda$. In each case, the results supported the position that the SNF of a given antenna allows the prediction of the SNF of antennas of different size. Thus by making computations for a particular antenna size, and generalizing the results to antennas of different sizes, the problems of data acquisition and presentation become manageable.

By using the above techniques only about 10,000 data points are required to describe the SNF of circular apertures which radiate pencil beams. This collection of data suffices for antennas whose distributions can be approximated as described above and whose size is arbitrary. A similar number of points is required for rectangular antennas. This data is tabulated in Volume II of this report.

The following section discusses in more detail the areas of investigation summarized above.

III. ANALYSIS OF WORK PROGRESS

A. Discussion of Antenna Fields

Three field regions are generally considered to be associated with an antenna. These are the Fraunhofer or far region, the Fresnel region, and the near region. These regions are usually defined in terms of approximations which are made in the integral solution for the diffraction field. For planar apertures (and hence, antennas whose radiating "aperture" can be considered planar), such as shown in Figure 1, the diffraction field is given by:

$$U_p = \frac{1}{4\pi} \int_{\text{Aperture}} F(\xi, \eta) \frac{e^{-jkr}}{r} \left[\left(jk + \frac{1}{r} \right) \vec{i}_z \cdot \vec{r}_1 + jk \right] d\xi d\eta \quad (1)$$

where

$F(\xi, \eta)$ is the aperture distribution

$k = 2\pi/\lambda$ is the wave number

\vec{i}_z is a unit vector in the z-direction

\vec{r}_1 is a unit vector in the direction of r .

As defined by Silver¹ the various field regions are:

1. Near Field Region. That region in the immediate neighborhood of the aperture in which no simplifying approximations can be made in Equation (1).

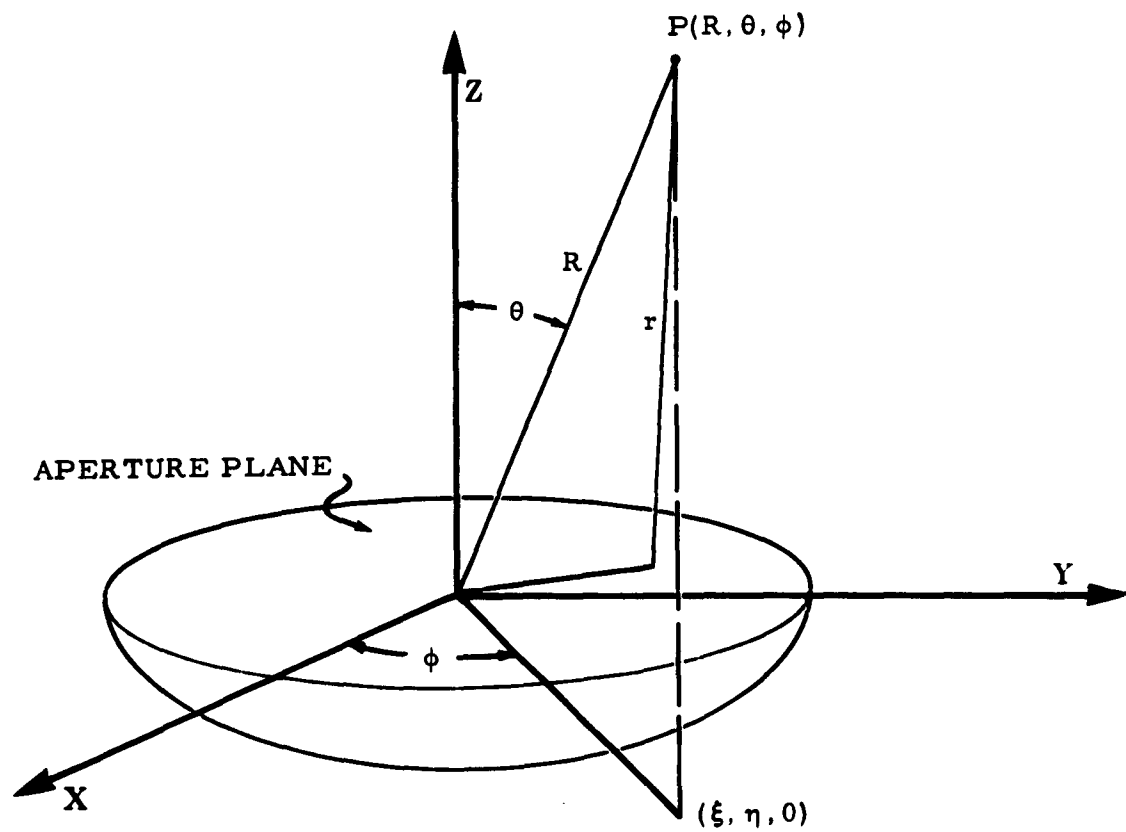


Figure 1. Coordinate Frame

2. Fresnel Region. In the Fresnel region several approximations are made; they are:

$$\left[\left(jk + \frac{1}{r} \right) \vec{i}_z \cdot \vec{r}_1 + jk \right] = jk(1 + \cos \theta)$$

$r = R$ in the amplitude term

$$r = R - \xi \sin \theta \cos \phi - \eta \sin \theta \sin \phi + \frac{1}{2R} \left[\xi^2 + \eta^2 - (\xi \sin \theta \cos \phi + \eta \sin \theta \sin \phi)^2 \right] \text{ in the phase term.}$$

Substituting the above approximations into Equation (1) yields for the Fresnel field,

$$U_p = (1 + \cos \theta) \frac{je^{-jkR}}{2\lambda R} \int_{\text{Aperture}} F(\xi, \eta) e^{jk \sin \theta (\xi \sin \phi + \eta \sin \phi)} \cdot e^{-\frac{jk}{2R} [\xi^2 + \eta^2 - \sin^2 \theta (\xi \cos \phi + \eta \sin \phi)^2]} d\xi d\eta \quad (2)$$

3. Fraunhofer Region. The approximations in the Fraunhofer region are the same as in the Fresnel region except for the approximation for the phase term. The phase term is taken to be

$$r = R - \xi \sin \theta \cos \phi - \eta \sin \theta \sin \phi$$

and the Fraunhofer field is

$$U_p = (1 + \cos \theta) \frac{j e^{-jkR}}{2\lambda R} \int_{\text{Aperture}} F(\xi, \eta) e^{jk \sin \theta (\xi \cos \phi + \eta \sin \phi)} d\xi d\eta \quad (3)$$

Care must be exercised in using Equations (1) to (3) for predicting the field associated with a radiating aperture. Besides the approximations listed above, approximations are made in the reduction of the vector solution for the field to a scalar solution as written in Equation (1). These approximations effectively discard the radial components of the field. These components give rise to stored energy which can be appreciable in the vicinity of the aperture, but which decays rapidly as the distance from the aperture is increased. Although little work has been done toward estimating the magnitude of the reactive fields, they are generally considered to be negligible in a region outside of a sphere bounding the aperture. Therefore, Equation (1) can be considered to give only qualitative results when applied to points interior to such a sphere.

The term "Fresnel region" is often used to encompass the entire region between the radiating aperture and the far field. The fact that the Fresnel approximations are not valid over this entire region has led to a large measure of confusion. In order to clarify the situation for the purpose of the present program, it is necessary to recognize the nature of and reasons for the various approximations. Both the Fresnel and Fraunhofer approximations are intended to render the integral solutions for the field amenable to simplified analysis and manipulation. In particular, when the Fraunhofer approximations are used in connection with a line source, the radiated field and the aperture distribution are related by a Fourier transformation. This is of great value when it is desired to synthesize a given Fraunhofer pattern. The Fresnel approximations do not

yield such a marked advantage, however, and only slightly simplify the form of the integrals. If the integrals are to be evaluated by the use of electronic computer techniques, as they were in the present program, the simplifications introduced by the Fresnel approximation are not great enough to warrant their use. Therefore, these approximations were not used in the program. The defining integral for the fields were taken to be

$$U_p = (1 + \cos \theta) \frac{j}{2\lambda} \int_{\text{Aperture}} F(\xi, \eta) \frac{e^{-jkr}}{r} d\xi d\eta \quad (4)$$

where no approximation for r were made.

Since Equation (4) yields a better approximation to the field than does the Fresnel formulation, it is improper to refer to the field calculated by use of Equation (4) as the Fresnel field. In order to clearly distinguish this field, it will be referred to as the scalar near field (SNF).

The region in which the scalar near field accurately represents the true field of an antenna extends from distances which are such that the radial components of field are negligible to infinity. However, since antennas are usually designed on the basis of the Fraunhofer approximations, it is desirable to consider the scalar near field as extending only to a distance at which these approximations are valid. The transition distance between the scalar near field and the Fraunhofer field is discussed in Section III. B.

In the region interior to the scalar near field, the radial components of field (and therefore the stored energy) are not negligible. To distinguish the field in this region from the scalar near field, it will be

referred to as the aperture field. To determine the transition distance between the aperture field and the scalar near field, the radial components of field (about which little is known) must be investigated. Although speculative, it is felt that this transition distance is approximately one antenna diameter from the aperture.

To summarize: In the present program the fields associated with an antenna are divided into three categories. They are defined below:

1. Aperture Field. The field in the immediate neighborhood of the aperture in which a scalar solution for the field is not necessarily valid. It extends outward from the aperture to a distance which is of the order of an antenna diameter.

2. Scalar Near Field. The field which exists in the region between the aperture field and the far field. A scalar solution is valid in this region; however, geometrical approximations for the distance term are not valid, especially near the inner boundary of this region.

3. Far Field. The field which extends from the outer boundary of the scalar near field to infinity. In the scalar solution, the approximation is made that rays emanating from all points on the aperture and traveling to a far field point travel along parallel paths.

B. Scalar Near Field to Far Field Transition Region

At sufficiently great distances, the scalar near field and Fresnel formulations are essentially identical. Therefore, the transition region between the scalar near field and the far field is the same as that between the Fresnel and far fields. The Fresnel-Fraunhofer transition distance is commonly taken to be $2L^2/\lambda$ where L is the longest linear dimension of the aperture and λ is the wavelength. Under this definition, the aperture appears to have a maximum phase error of $\pi/8$ at its extreme edge. This criterion is extremely simple to apply, for under it all antennas which have the same maximum dimension have the same Fresnel-Fraunhofer transition distance.

However, to be meaningful from an interference viewpoint, the criterion for the transition distance should be based on limiting the degradation in the radiation pattern. The degree of degradation depends on the aperture shape and the distribution function, as well as on the antenna size and the distance between the antenna and the observation point. This has been demonstrated in the literature for the case of on-axis fields.^{2,3} A transition distance criterion based upon the on-axis field is not general enough, however, since in many applications (including interference) the off-axis power distribution is of extreme importance.

Experience indicates that the first significant effect of moving into the Fresnel field is a filling of the nulls in the Fraunhofer radiation pattern. This is accompanied by a slight increase in the level of the sidelobes immediately adjacent to the main beam. Further in the Fresnel field, the sidelobes are gradually enveloped by the main beam. At a given distance, these effects become more prominent as the antenna's sidelobe level

is lowered, indicating that the transition distance moves outward as the distribution becomes tapered. This general behavior is substantiated by the calculations of Hansen and Bailin,⁴ and is illustrated in Figure 2. Figure 2 shows the calculated Fraunhofer pattern and the pattern shape at a distance $R = 2L^2/\lambda$, of a very low sidelobe (-50 db) Tchebyscheff array made of nine elements. It is noted that the first sidelobe is completely enveloped by the main beam at the distance $R = 2L^2/\lambda$, which corresponds to the standard far field distance. However, the levels of the succeeding sidelobes are not substantially altered. Although a -50 db Tchebyscheff array is an extreme case and of limited practical importance, it serves to point out that the transition distance, under certain conditions, can be greater than $2L^2/\lambda$. It also shows that the accuracy of the Fraunhofer approximations, with respect to predicting the field strength at a point, depends upon the azimuthal location of the point, as well as the distance between the point and the antenna.

Since null-filling is the first significant effect of moving into the Fresnel field, it is logical to base the transition distances on a criterion which limits the degree to which the various nulls are filled. Under this criterion, the Fresnel field in the direction of the n^{th} far field zero (numbering from the main beam outward) is limited to a percentage K, of the n^{th} sidelobe level. Thus, by determining the transition distance for various values of n, and relating n to the azimuth angle, the transition distance is determined as a function of angle. To determine the effect of such factors as the aperture shape and distribution function, a number of different distributions have been investigated. The distributions chosen for investigation were Bickmore and Spellmire's two-parameter family of line sources,⁵ Taylor's line source distribution which yields an arbitrary number of equal sidelobes,⁶ and Taylor's circular aperture distribution which also yields

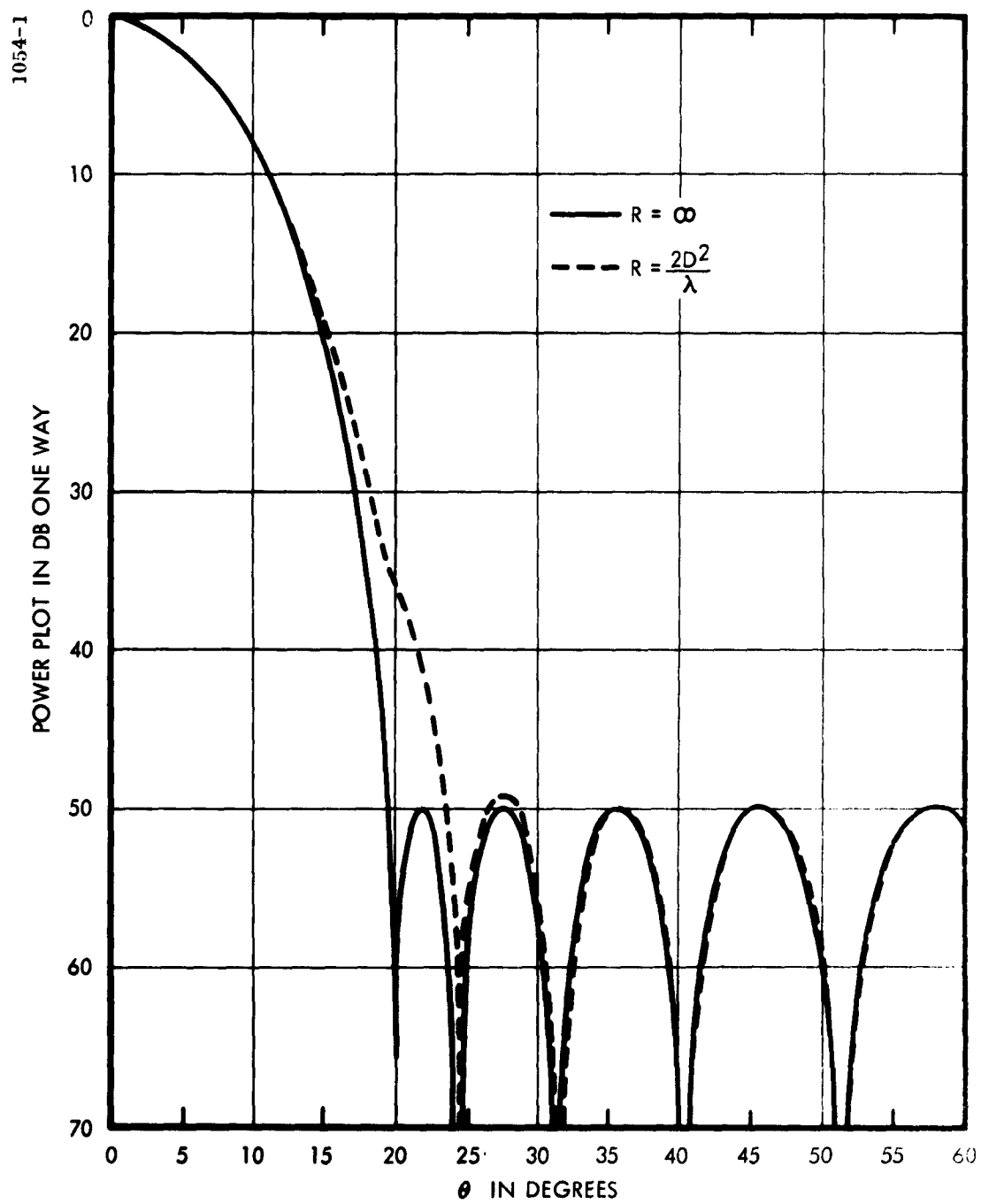


Figure 2. Calculated Field of Nine-Element Tchebyscheff Array

an arbitrary number of equal sidelobes.⁷ The results of the investigations of the latter two distributions are in substantial agreement, and only those for the line source are presented herein.

Before proceeding to the mathematical details of the analysis, a short discussion of the procedure used will be presented. For the purposes of clarity, it is convenient to anticipate some of the results of the analysis in the course of this discussion. Each of the above classes of distribution contains a parameter that controls the sidelobe levels of the corresponding radiation patterns. Additionally, Bickmore and Spellmire's family contains a parameter which controls the sidelobe taper. Thus, the dependence of the transition distance on both the sidelobe level and taper can be determined by investigating the above distributions.

Because of the mathematical complexities of Fresnel field investigations, it was expedient to use an approximate analysis in the transition distance investigations. The approximate analysis has indicated that the first null transition distance is highly dependent upon the sidelobe level, and to a lesser extent dependent upon the sidelobe taper. It also indicates that as n increases the dependence on the sidelobe level decreases, but the dependence on the sidelobe taper becomes more pronounced; these conclusions were reached under the condition that the degree of null filling, specified by K , is identical for each family of distributions. Because of the questionable validity of the analysis for values of $n > 1$, the validity of these conclusions was further investigated, using a more exact analysis. The more exact analysis has supported the position that for values of $n > 3$, the n^{th} -null transition distance is virtually independent of the sidelobe level, as was predicted by the approximate analysis. This result is fortuitous since it allows an entire family of distributions to be investigated, simply

by investigating a particular distribution belonging to that family. A nearly exact determination of the Fresnel field was made for two particular distributions each belonging to a different family in order to ascertain the effect of the sidelobe taper on the transition distance. The results of the latter analysis indicate that if the sidelobes decay slowly, K must be selected as a descending function of n in order for the results of the transition distance analysis to be valid. However, if the sidelobes decay rapidly, K may be taken to be independent of n . When K is appropriately modified the n^{th} -null transition distance becomes virtually independent of sidelobe taper as well as the sidelobe level. For large n , it varies as $L/\sin \theta$, where L is the antenna length and θ the angle from broadside. The transition distance analysis follows.

Because of the similarity between the analyses of each of the previously mentioned distributions only one distribution will be treated in detail. At the outset it is advantageous to consider a rectangular aperture with an arbitrary distribution function.

The Fresnel field for a rectangular aperture of dimensions L_1 , L_2 , is given by

$$U(R, \theta, \phi) = \int_{-L_1/2}^{L_1/2} \int_{-L_2/2}^{L_2/2} G(\xi, \eta) e^{jk \sin \theta (\xi \cos \phi + \eta \sin \phi)} \\ \cdot e^{-\frac{jk}{2R} [\xi^2 + \eta^2 - \sin^2 \theta (\xi \cos \phi + \eta \sin \phi)^2]} d\xi d\eta \quad (5)$$

where (ξ, η) are the aperture coordinates, $G(\xi, \eta)$ is the aperture distribution, $k = 2\pi/\lambda$ is the wave number, and (R, θ, ϕ) are the standard spherical coordinates. For separable distributions $G(\xi, \eta) = G(\xi) G(\eta)$. For such distributions and in the (ξ) principal plane ($\phi = 0$), Equation (5) may be written

$$U(R, \theta, \phi) = \int_{-L_2/2}^{L_2/2} G(\eta) e^{\frac{jk\eta^2}{2R}} d\eta \cdot \int_{-L_1/2}^{L_1/2} G(\xi) e^{jk\xi \sin \theta} e^{-\frac{jk}{2R} \xi^2 \cos^2 \theta} d\xi \quad (6)$$

It is seen from Equation (6) that the η integration does not affect the shape of the pattern in the $\phi = 0$ plane. Therefore, the transition distance can be analyzed on the basis of a line source. For $R \gg L_1$, the quadratic phase term in the second integral of Equation (6) may be approximated by

$$e^{-\frac{jk}{2R} \xi^2 \cos^2 \theta} \approx 1 - \frac{jk}{2R} \xi^2 \cos^2 \theta \quad (7)$$

As mentioned previously, the approximation of Equation (7) will restrict K to be a decreasing function of n for distribution functions that give rise to patterns whose sidelobes decay slowly.

Inserting Equation (7) into Equation (6), dropping the η integration, and writing $L_1 = L$ yields

$$U(R, \theta, \phi) = \int_{-L/2}^{L/2} G(\xi) e^{jk\xi \sin \theta} d\xi - \frac{jk \cos^2 \theta}{2R} \int_{-L/2}^{L/2} \xi^2 G(\xi) e^{jk\xi \sin \theta} d\xi \quad (8)$$

The first integral of Equation (8) is the far field of the line source and the second integral is the error field introduced by operating in the Fresnel region. In the directions in which the Fraunhofer field vanishes, θ_n , the error field is given approximately by

$$E(\theta_n) = \frac{k}{2R} \int_{-L/2}^{L/2} \xi^2 G(\xi) e^{jk\xi \sin \theta_n} d\xi \quad (9)$$

Under the change of variables $P = \frac{2\pi\xi}{L}$, $u_n = \frac{L}{\lambda} \sin \theta_n$, the error field relative to the peak of the Fraunhofer pattern is

$$E(u_n) = \frac{1}{4\pi} \left(\frac{L^2}{\lambda R} \right) \frac{\int_{-\pi}^{\pi} p^2 G(p) e^{ju_n p} dp}{\int_{-\pi}^{\pi} G(p) dp} \quad (10)$$

The Fresnel-Fraunhofer transition distance is established by setting $E(u_n)$ equal to a percentage of the n^{th} sidelobe ratio.

$$E(u_n) = \frac{K}{S_n} \quad (11)$$

where S_n is the voltage ratio of the main beam to the n^{th} sidelobe, and K is a parameter which establishes the degree of null-filling. Substituting Equation (11) into Equation (10) and rearranging, yields

$$\frac{K\lambda R}{L^2} = \frac{S_n}{4\pi} \frac{\int_{-\pi}^{\pi} p^2 G(p) e^{ju_n p} dp}{\int_{-\pi}^{\pi} G(p) dp} \quad (12)$$

The transition distance, R , can be obtained from Equation (12) if the distribution function, $G(p)$, and its corresponding far field pattern is known. To illustrate the technique, Bickmore's two-parameter family of line source distributions will be considered. This family of distributions is given by

$$G(p) = \frac{1}{2\pi} \left[\frac{\sqrt{\pi^2 - p^2}}{i\pi C} \right]^{\nu-1/2} J_{\nu-1/2} \left(iC \sqrt{\pi^2 - p^2} \right), \quad |p| < \pi$$

$$G(p) = 0, \quad |p| > \pi \quad (13)$$

These distributions are particularly useful because the parameters C and ν control the sidelobe level and the sidelobe decay rate, respectively; these factors, in turn, most strongly influence the transition distance. In general, as C increases the sidelobes decrease, and as ν increases the sidelobe decay rate increases. For $\nu < 1/2$, the distributions become infinite at

the extremes of the aperture, and thus they possess no physical counterparts. For $\nu = 1/2$, the distributions are finite at the aperture extremes and for $\nu > 1/2$ the distributions vanish there. The present example will be restricted by choosing $\nu = 1/2$, which corresponds to the case most often encountered in practice. For $\nu = 1/2$, the distributions of Equation (13) become

$$G(p) = \frac{1}{2\pi} J_0 \left(iC \sqrt{\pi^2 - p^2} \right) , \quad |p| < \pi$$

$$G(p) = 0 , \quad |p| > \pi$$
(14)

The corresponding far field pattern is obtained by a Fourier inversion of Equation (13) and is given by

$$F(u) = \frac{\sin \pi \sqrt{u^2 - C^2}}{\pi \sqrt{u^2 - C^2}}$$
(15)

This class of patterns has also been studied by Taylor⁸ and is often referred to as modified $\frac{\sin u}{u}$ type patterns. As indicated previously, the sidelobe level is controlled by the parameter C . The decay rate is fixed however, since $\nu = 1/2$. The sidelobe taper (ratio of the first to the second sidelobe) is 4.5 db. The zeros of the pattern, u_n , occur at

$$u_n = \sqrt{n^2 + C^2} , \quad n = 1, 2, 3, \dots$$
(16)

and the maxima of the pattern are given by $\gamma_{3/2,n}$, where

$$\gamma_{3/2,n} = n^{\text{th}} \text{ root of } J_{3/2}(x) = 0$$
(17)

Noting that

$$S_n = \frac{F(0)}{F(\gamma_{3/2,n})} \quad (18)$$

and

$$\int_{-\pi}^{\pi} G(p) dp = F(0) \quad (19)$$

It is seen that

$$\frac{S_n}{\int_{-\pi}^{\pi} G(p) dp} = \frac{1}{F(\gamma_{3/2,n})} = \frac{\gamma_{3/2,n}}{\sin(\gamma_{3/2,n})} \quad (20)$$

Inserting Equations (16) and (20) into Equation (12) yields

$$\frac{K\lambda R}{L^2} = \frac{1}{8\pi^2} \frac{\gamma_{3/2,n}}{\sin(\gamma_{3/2,n})} \int_{-\pi}^{\pi} p^2 J_0^2(iC\sqrt{\pi^2 - p^2}) e^{ju_n p} dp \quad (21)$$

where u_n and $\gamma_{3/2,n}$ are obtained from Equations (16) and (17), respectively.

Equation (21) was evaluated numerically for values of n equal to 1, 2, and 3. The results are shown in Figure 3; these results clearly show that the first null criterion yields a transition distance which is significantly greater than the transition distances obtained by using criteria based upon succeeding higher nulls as well as by other criteria. This supports

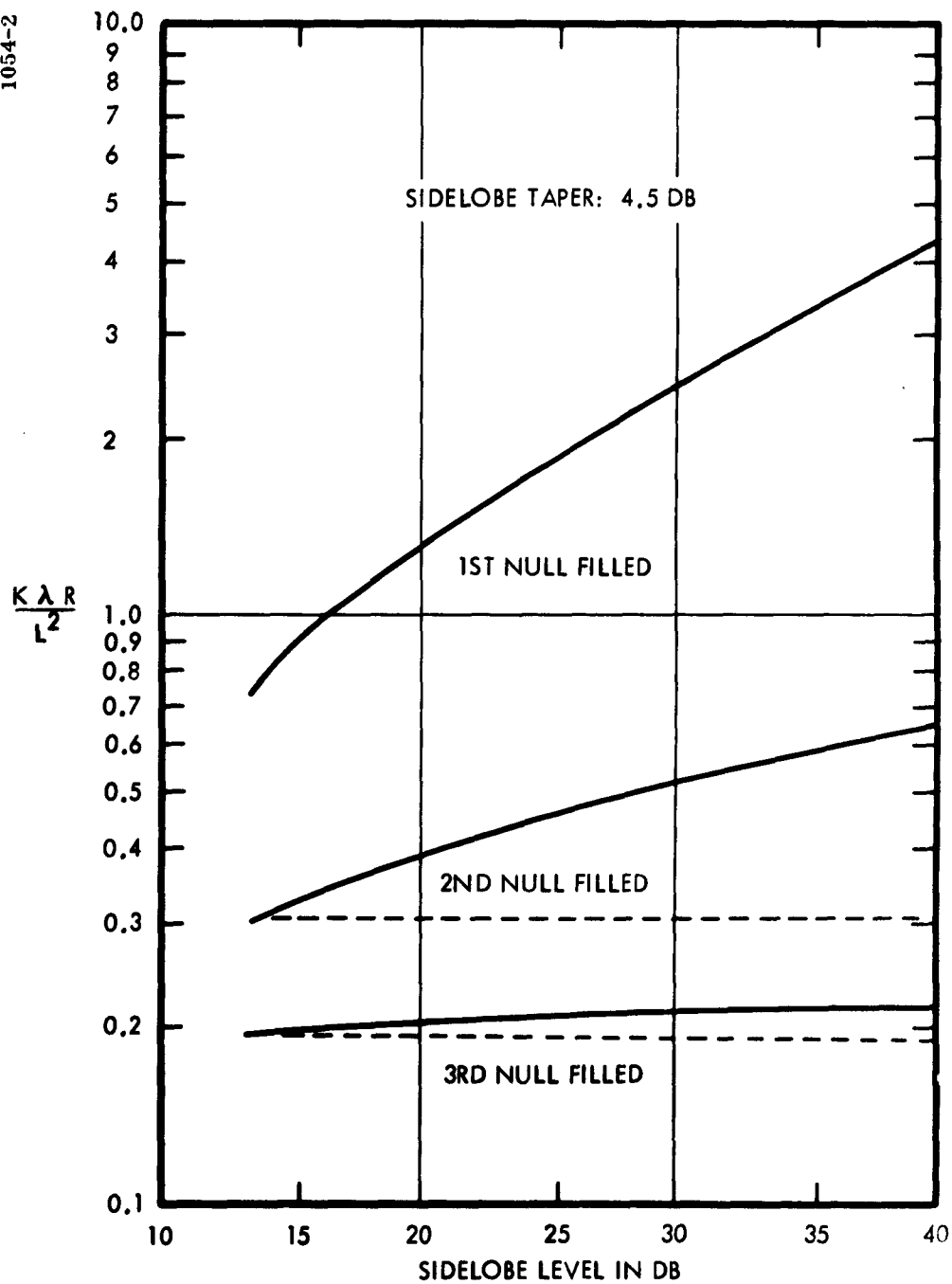


Figure 3. Transition Distance — 4.5 db Sidelobe Taper

the previous argument that the Fraunhofer formulation can be used to estimate the field strength for sufficiently wide angles at distances significantly closer than $2L^2/\lambda$.

Figure 3 also indicates that as n increases the corresponding transition distance becomes less dependent upon the sidelobe level. This can also be demonstrated analytically. Equation (21) is integrated in Appendix I for large n , and the asymptotic representation for the transition distance is obtained as:

$$\frac{K\lambda R}{L^2} \sim \frac{2n+1}{4n^2} \quad (22)$$

Equation (22) which is independent of C and therefore of the sidelobe level, is shown for $n = 2$ and $n = 3$ as the dashed lines on Figure 3. The agreement between the transition distance calculated by use of Equations (21) and (22) is very good for the value $n = 3$. Therefore, the transition distances corresponding to higher values of n can be obtained by use of Equation (22).

An analysis identical to that presented above was performed for the distribution functions of Equation (13), for a value of $\nu = 3/2$. These functions yield patterns whose sidelobe tapers are approximately 7.6 db. The results of this analysis are shown in Figure 4. Again it is seen that as n increases the transition distance decreases. Figure 5 shows the $n = 1$ and $n = 2$ transition distances for Taylor line sources, which yield equal sidelobe levels. Figure 6 summarizes the effect of varying the sidelobe level and taper on the first null transition distance. The transition distance of distributions whose sidelobe tapers lie between zero db and 8 db lie within the shaded region. Therefore, this curve can be used to estimate the

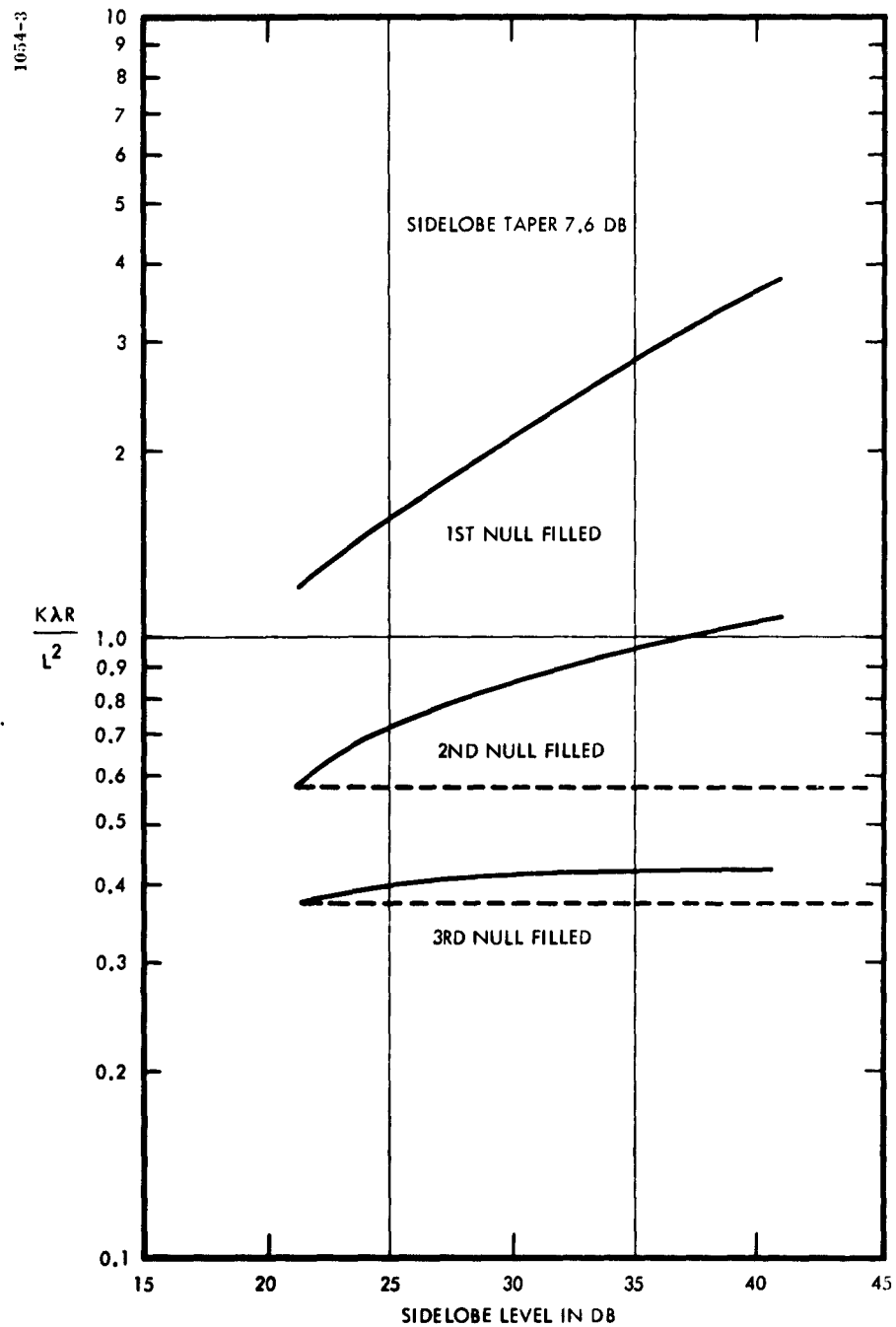


Figure 4. Transition Distance — 7.6 db Sidelobe Taper

1054-4

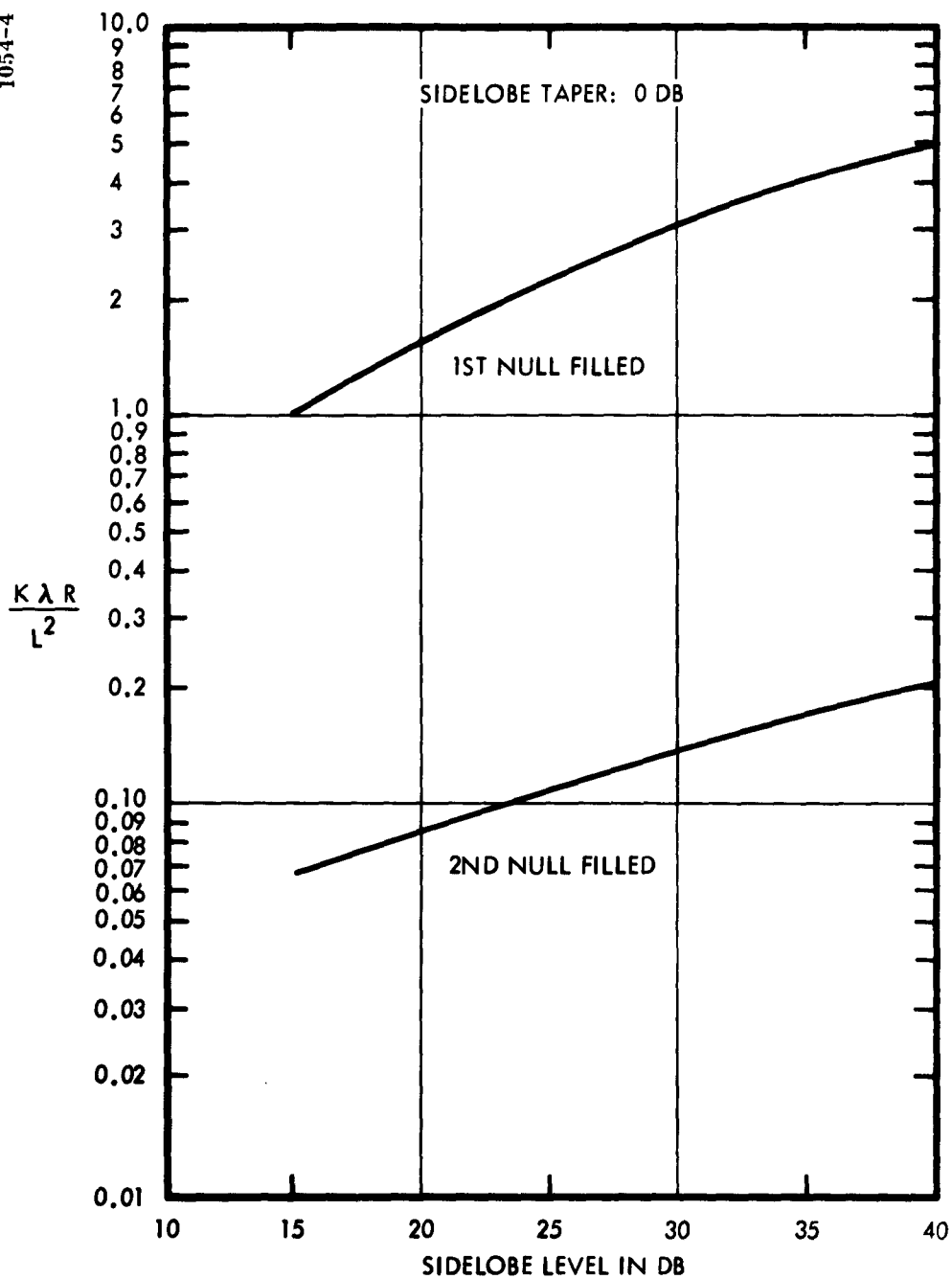


Figure 5. Transition Distance — 0 db Sidelobe Taper

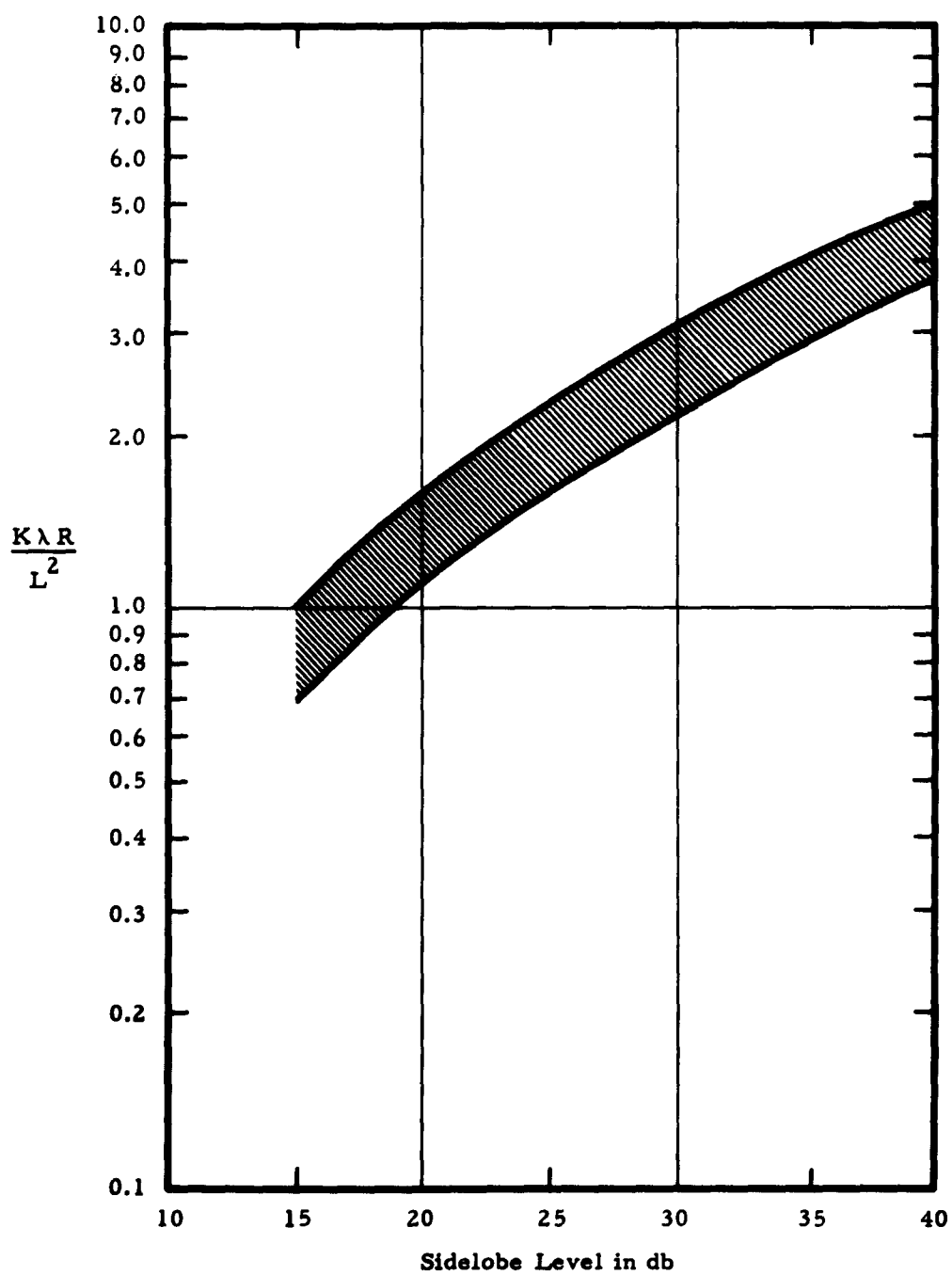


Figure 6. Variation in First Null Transition Distances

transition distance of most pencil beam type antennas encountered in practice. If the antenna whose first null transition distance is to be estimated has no sidelobe taper (for example, a Dolph-Tchebyscheff array), its transition distance will follow the upper boundary of the shaded region of Figure 6. If the sidelobe taper is 8 db, the transition distance approximately follows the lower boundary. For intermediate tapers, the transition distance can be estimated by interpolation.

Inspection of Figures 3, 4, and 5 indicates that as the sidelobe taper increases, the first-null transition distance decreases but that the second and higher-null transition distances increase. In fact, for large n , the asymptotic expression for the transition distance for the case $\nu = 3/2$ is

$$\frac{K\lambda R}{L^2} \sim \frac{(n+1)^2}{(n+1/2)^3} \quad (23)$$

Comparison of Equations (22) and (23) indicates that for large n the transition distance for the family of distributions given by $\nu = 3/2$ is approximately twice that for the family given by $\nu = 1/2$. The shortening of the higher-null transition distances appears to be even more marked for the Taylor line sources, for which the sidelobe taper is zero db. However, the values of the transition distances as given by Figures 3, 4, and 5 or by Equations (22) and (23), do not satisfy the approximation of Equation (7) unless K is taken to be less than $1/n$. Therefore, the results of the analyses are questionable for $n > 1$, unless K is suitably restricted.

It will now be shown that as the sidelobe taper decreases, the restrictions on K become more severe. This results in the transition distance becoming independent of the sidelobe taper for large n . To determine

the restrictions on K under which Equations (22) and (23) are valid, Equation (6) must be integrated without the use of the approximation of Equation (7). This will be done for the cases of $\nu = 1/2$ and $\nu = 3/2$. Since Equations (22) and (23) are independent of the value πC , it suffices to perform the integrations for the special case of $\pi C = 0$. For a uniform distribution ($\nu = 1/2$, $\pi C = 0$) the second integral of Equation (6) may be written in terms of Fresnel integrals. This is accomplished by completing the square in the exponential, using the change of variables,

$$Q = \frac{L^2}{4\pi\lambda R} \cos^2 \theta$$

$$u = \frac{L}{\lambda} \sin \theta \quad (24)$$

$$t = Q \left(\frac{2\pi\xi}{L} - \frac{u}{2Q} \right)^2$$

and noting,

$$\left(\frac{2}{\pi t} \right)^{1/2} \cos t = J_{-1/2}(t) \quad , \quad \left(\frac{2}{\pi t} \right)^{1/2} \sin t = J_{1/2}(t) \quad (25)$$

The second integral of Equation (6) then becomes:

$$E(Q, u) = -j \exp \left(\frac{ju^2}{4Q} \right) \left(\frac{\pi}{2Q} \right)^{1/2}$$

$$\cdot \frac{1}{2} \int_{Q(\pi - u/2Q)^2}^{Q(\pi + u/2Q)^2} \left[J_{-1/2}(t) + jJ_{1/2}(t) \right] dt \quad (26)$$

The integrals of Equation (26) are Fresnel's integrals $C(x)$ and $S(x)$, respectively, which are tabulated. Thus, Equation (26) allows the exact evaluation of $E(Q, u)$. To determine the value of the Fresnel field at the n^{th} -null transition distance, the corresponding values of Q and u must be ascertained. From Equation (16), it is seen that in the direction of the n^{th} far field zero, $u = n$. Q is obtained from Equations (22) and (24); neglecting the factor $\cos^2 \theta$:

$$Q = \frac{Kn^2}{\pi(2n + 1)} \quad (27)$$

By inserting $u = n$ and Equation (27) into Equation (26), the exact value of the field is calculated in the direction of the n^{th} -null transition distance.

The approximate and the exact values of the Fresnel field have been calculated from Equations (22) and (26) respectively, as a function of K for values of $n = 1, 2, 3, 10$, and 25 ; the results are shown in Figure 7, in which the solid curves represent the exact field values and the dashed lines represent the approximate values. The agreement is very good in all cases if K is sufficiently less than unity. However, as n decreases, the maximum value of K may increase without degrading the accuracy of the results. For $n = 1$, K may take on values of unity or even larger. Hence, for the distribution under consideration, it is reasonable to select K as a decreasing function of n . In this way, the results for all n have approximately the same accuracy. A reasonable choice of the functional relationship can be made by considering the asymptotic limits of the Fresnel integrals.

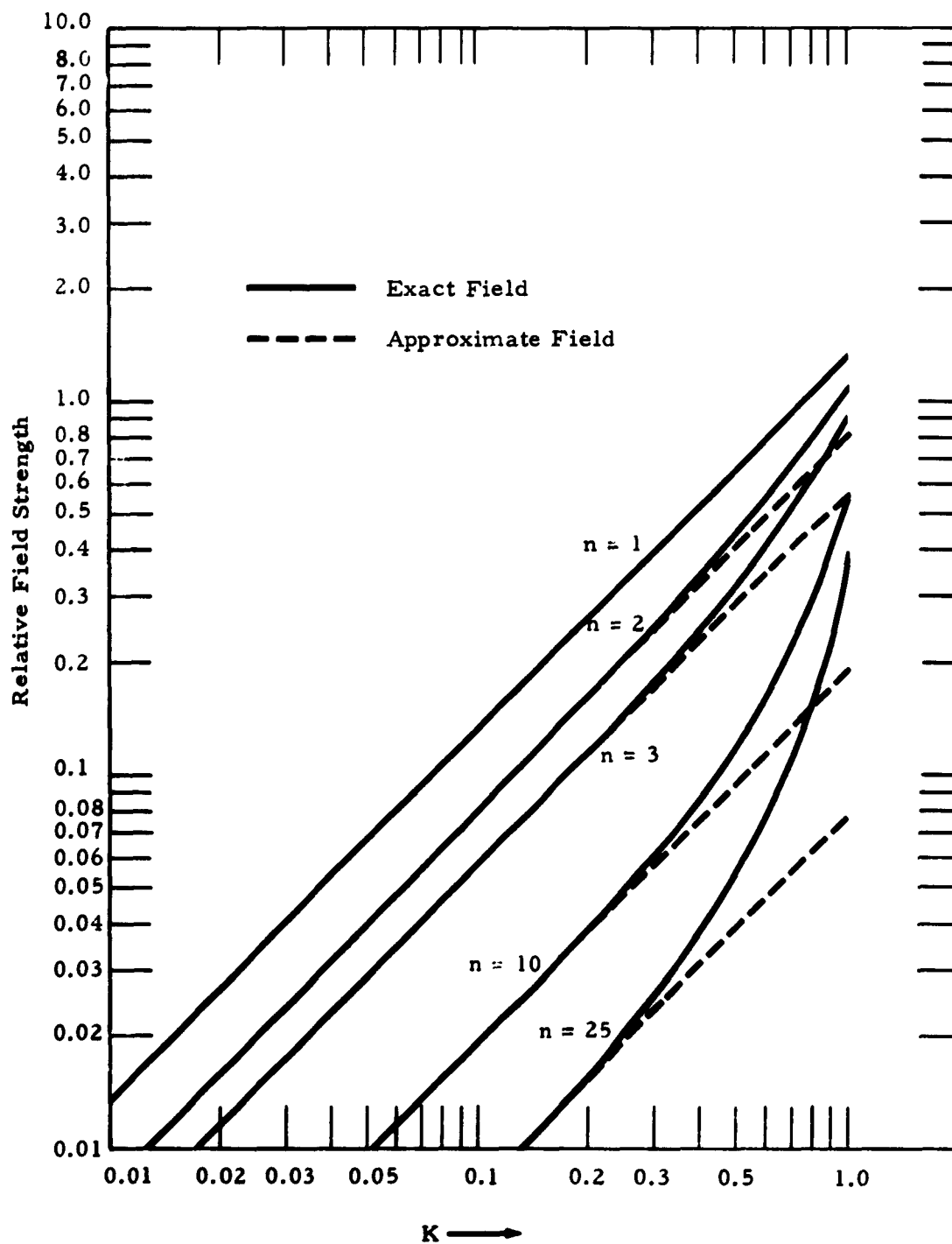


Figure 7. Fresnel Field Strength in Direction of Far Field Zeros and at the Transition Distance — Uniform Distribution

$$(1/2) \int_0^x J_{-1/2}(t) dt \sim 1/2 + \frac{\sin x}{\sqrt{2\pi x}} + O\left(\frac{1}{2\pi x}\right) \quad (28)$$

$$(1/2) \int_0^x J_{1/2}(t) dt \sim 1/2 - \frac{\cos x}{\sqrt{2\pi x}} + O\left(\frac{1}{2\pi x}\right)$$

Inserting $u = n$ and Equation (27) into Equation (26) and using Equation (28) yields after some manipulation, the following asymptotic representation for the exact field

$$E(K, n) \sim \frac{4K(2n+1)}{(2n+1)^2 - (2Kn)^2} \quad (29)$$

The approximate value of the Fresnel field is given by

$$E(K, n) = \frac{K}{S_n} \sim \frac{4K}{2n+1} \quad (30)$$

Subtracting Equation (30) from Equation (29) and dividing by Equation (29) yields the error introduced by the approximation of Equation (7). The error is simply K^2 . Thus, a value of $K = 1/2$ yields an error of only 25 percent in the calculation of the field strength in the directions of the localized minima. The error in the direction of the localized maxima is significantly less. Hence, a reasonable selection for K , as a decreasing function of n , is

$$K = \frac{n+1}{2n} \quad (31)$$

which is unity for $n = 1$, and approaches $1/2$ as n approaches infinity. Substituting Equation (31) into (22) yields the transition distance

$$R = \frac{2n + 1}{2n(n + 1)} \frac{L^2}{\lambda} \quad (32)$$

which is valid for all values of n . It is noted that for n large (i. e., the azimuthal angle large with respect to an antenna beamwidth), Equation (32) reduces to

$$R = \frac{L^2}{n\lambda} = \frac{L}{\sin \theta} \quad (33)$$

Equation (6) may be integrated without the use of the approximation of Equation (7) for the distribution specified by $\nu = 3/2$, $\pi C = 0$ (which corresponds to an aperture distribution of $\pi^2 - p^2$), by successive integration by parts. Although this process is tedious, it is straightforward and will be omitted for the purposes of brevity. When the exact and approximate values of the Fresnel field are compared in a manner similar to the above, it is found that K may be taken as unity regardless of n , with approximately equal results. Substituting unity for K into Equation (23), the transition distance may be written as

$$R = \frac{(n + 1)^2}{(n + 1/2)^3} \frac{L^2}{\lambda} \quad (34)$$

which again reduces to,

$$R = \frac{L}{\sin \theta} \quad (35)$$

for n large. Thus, it can be concluded that for azimuthal angles which are large compared to an antenna beamwidth, the transition distance is nearly independent of the distribution function.

C. SNF of Circular Apertures

1. Mathematical Formulation

The scalar near field of a planar circular aperture of radius a , illuminated by a circularly-symmetric distribution function, may be written from Equation (4) as

$$F_N(R, \theta) = (1 + \cos \theta) \frac{ja^2}{2\lambda} \int_0^{2\pi} \int_0^1 f(\rho) \frac{e^{-jkr}}{r} \rho d\rho d\beta \quad (36)$$

where

$$r = \sqrt{R^2 + a^2 \rho^2 - 2a\rho R \sin \theta \cos(\phi - \beta)}$$

By the addition theorem for spherical Bessel functions, we may write

$$\frac{e^{-jkr}}{r} = jkh_0^{(2)}(kr) = jk \sum_{n=0}^{\infty} (2n+1) P_n[\sin \theta \cos(\phi - \beta)] j_n(ka\rho) h_n^{(2)}(kR) \quad (37)$$

$$R > a$$

where $h_n^{(2)}(kR)$ is the spherical Hankel function of the second kind, $j_n(ka\rho)$ is the spherical Bessel function and $P_n[\sin \theta \cos(\phi - \beta)]$ is the Legendre polynomial. The only factor containing the β coordinate is the Legendre

polynomial. The β integral can be performed with the aid of the addition theorem for Legendre polynomials.

$$P_n[\sin \theta \cos(\phi - \beta)] = P_n(0) P_n(\cos \theta) + 2 \sum_{m=1}^{\infty} \frac{(n-m)!}{(n+m)!} P_n^m(0) P_n^m(\cos \theta) \cos m(\phi - \beta) \quad (38)$$

where $P_n^m(\cos \theta)$ is the associated Legendre polynomial. Because of the factor $\cos m(\phi - \beta)$, each term in the infinite series of Equation (38) vanishes when integrated over β through the range 2π . Therefore

$$\int_0^{2\pi} P_n(\sin \theta \cos \beta) d\beta = 2\pi P_n(0) P_n(\cos \theta) \quad (39)$$

The scalar near field is then given by

$$F_n(R, \theta) = \frac{1 + \cos \theta}{2} jka^2 \sum_{n=0}^{\infty} (2n+1) P_n(0) P_n(\cos \theta) h_n^{(2)}(kR) \int_0^1 f(\rho) j_n(ka\rho) \rho d\rho \quad (40)$$

where

θ = off-axis angle

a = antenna radius

$k = 2\pi/\lambda$ = the wave number

$f(\rho)$ = aperture distribution

$P_n(x)$ = Legendre polynomial

$h_n^{(2)}(x)$ = spherical Hankel function of the second kind

$j_n(x)$ = spherical Bessel function

The formulation of Equation (40) is particularly useful because of the fact that the included integral is independent of the coordinates (R, θ) of the field point. Thus, for a given antenna this integral need be evaluated only once. When this is accomplished, the series can be summed for various choices of (R, θ) in order to determine the spatial distribution of energy.

Although this series formulation is, of course, amenable to computer techniques, the evaluation of Equation (40) is complicated by the fact that numerical values of the spherical Bessel and Hankel functions are not available for the range of orders required. Briefly, large orders are required for the following reasons: For large values of ka (large antennas), the argument of the spherical Bessel function in the integral of Equation (40) becomes large near $\rho = 1$. This integral decreases for sufficiently large n , and as a result governs the convergence of the series. Approximately $1.2 ka$ terms are required for convergence; thus, spherical functions of very high order must be retained. For example, approximately 1100 terms are required to evaluate the expression for an antenna whose diameter is 300 wavelengths. Thus, a knowledge of the spherical functions for at least this order is required. However, previous to the present program, numerical data was not available for orders greater than about 60. To overcome this difficulty a subprogram for determining the values of these functions, and for evaluating the integral of Equation (40) was required. This program is discussed briefly below.

2. Computer Program

The programs for determining the spherical Hankel and Bessel functions were written in a manner which minimized the computation time, and thus the cost. The first step in the program was to relate the spherical Bessel functions to the cylindrical Bessel functions as follows:

$$j_n(x) = \sqrt{\frac{\pi}{2x}} J_{n+1/2}(x) \quad (41)$$

$$h_n^{(2)}(x) = \sqrt{\frac{\pi}{2x}} H_{n+1/2}^{(2)}(x) \quad (42)$$

Here $J_\nu(x)$ is the Bessel function of the first kind commonly referred to simply as the Bessel function, and $H_\nu^{(2)}(x)$ is the Bessel function of the third kind, commonly referred to as the Hankel function. The Hankel function is related to the cylindrical Bessel functions of the first and second kinds by

$$H_\nu^{(2)}(x) = J_\nu(x) - jN_\nu(x) \quad (43)$$

Thus by evaluating the cylinder functions $J_\nu(x)$ and $N_\nu(x)$, the values of the spherical Bessel functions can be ascertained. In evaluating the cylinder functions, extensive use is made of the recurrence relation

$$C_{\nu+1}(x) = \frac{2\nu}{x} C_\nu(x) - C_{\nu-1}(x) \quad (44)$$

which is satisfied by both $J_\nu(x)$ and $N_\nu(x)$ as well as $H_\nu^{(2)}(x)$. For a given value of the argument, the function $N_\nu(x)$ can be evaluated for large ν from a knowledge of values for small ν , by Equation (44). This technique is of

limited value for evaluating $J_\nu(x)$, because these functions become very small for large ν and sufficient accuracy cannot be retained with available techniques. Thus, a more sophisticated program is required to evaluate $J_\nu(x)$. This program encompasses a number of techniques, the details of which are outlined in Appendix II.

Once the spherical Bessel and Hankel functions have been obtained, the integral of Equation (40) can be evaluated numerically. However, to obtain acceptable accuracy, the integral must be divided into 3 ka intervals. Since the number of terms required for convergence is also proportional to ka, the time for evaluating Equation (40) is proportional to $(ka)^2$, by this technique. For even moderately large apertures the computer time becomes prohibitive. This difficulty was overcome by establishing a recursion relationship satisfied by the integral of Equation (40), under the condition that the aperture distribution is of the form, $f(\rho) = 1 + a_1 \rho^2 + a_2 \rho^4 + a_3 \rho^6$. Under this condition the integrals involving odd orders of the spherical Bessel function are zero, and those involving even orders satisfy

$$\int_0^1 \rho^{2m+1} j_{2n}(k\rho) d\rho = \frac{4n+3}{2(n+m+1)} \frac{j_{2n+1}(k\rho)}{k\rho} - \frac{2(n-m)+1}{2(n+m+1)} \int_0^1 \rho^{2m+1} j_{2n+2}(k\rho) d\rho \quad (45)$$

It proved advantageous to apply Equation (45) in a backward manner; that is, the values of the integrals involving smaller orders of $j_{2n}(k\rho)$ were obtained from the values of the integrals involving large orders. By starting with a sufficiently large order, the integral on the righthand side of Equation (45) can be made arbitrarily small and can be taken to be zero. Inspection

of Equation (45) shows that when this procedure is followed, no integral need be evaluated directly. Thus, the required computer time was reduced by a factor of 3 ka from that of the more conventional approach. The accuracy of this approach was checked by comparing the results of calculations made on relatively small antennas, to those obtained by numerical integration. The two sets of data agreed to five places. The calculations were made on an IBM 7090 computer.

3. Evaluation of the SNF

With the aid of the computer program described above, the SNF of various antennas was readily calculated. In keeping with the philosophy of the study program, which was to obtain information that can readily be used to evaluate situations that arise in practice, a class of distribution functions capable of closely approximating practical aperture distributions was selected for study. These functions have the form $f(\rho) = 1 + a_1 \rho^2 + a_2 \rho^4 + a_3 \rho^6$. If, in a given situation, the aperture distribution is known, or can be measured, it can be matched by the above class of functions by appropriately selecting the aperture distribution parameters a_1 , a_2 , and a_3 . In the case of high-gain, paraboloidal-type reflectors, experience indicates that the primary feed patterns are usually quadratic in nature. Thus, if at some point the primary pattern's beamwidth is known (for example, the 3 db beamwidth), the distribution function can be predicted with reasonable accuracy. This phenomena is discussed more fully by Jasik,⁹ who presents universal feed horn patterns.

Using the technique of Jasik, which also accounts for the space attenuation factor, it is thus possible to obtain curves which relate the aperture distribution parameters a_1 , a_2 , and a_3 to the aperture taper.

(The aperture taper is the ratio of currents at the center and edge of the aperture.) Such curves are shown in Figure 8. The universal curves of Figure 8 are somewhat dependent upon the ratio of the focal length to antenna diameter (f/D ratio); the dependence is so slight that it can be ignored in most practical cases, however. The curves of Figure 8 were calculated for an f/D ratio of 0.400.

By inserting the function $1 + a_1 \rho^2 + a_2 \rho^4 + a_3 \rho^6$ for the distribution function $f(\rho)$, the integral of Equation (40) can be divided into four integrals as follows:

$$\begin{aligned} \int_0^1 f(\rho) j_n(k\rho) \rho d\rho = & \int_0^1 j_n(k\rho) \rho d\rho + a_1 \int_0^1 \rho^2 j_n(k\rho) \rho d\rho \\ & + a_2 \int_0^1 \rho^4 j_n(k\rho) \rho d\rho + a_3 \int_0^1 \rho^6 j_n(k\rho) \rho d\rho \end{aligned} \quad (46)$$

Each of the above integrals is purely real, as are each of the coefficients of the summation of Equation (40) except the spherical Hankel function. The spherical function is complex, as indicated by Equations (42) and (43), and thus the scalar near field is also complex.

The scalar near field for circular antennas of diameters 10λ , 20λ , 40λ , 80λ , and 160λ have been computed from Equation (40), for selected values of range. In the computations, the scalar near field was divided into eight components; four real and four imaginary. One real and one imaginary component arise from each of the integrals of Equation (46). Thus, the scalar near field takes the form

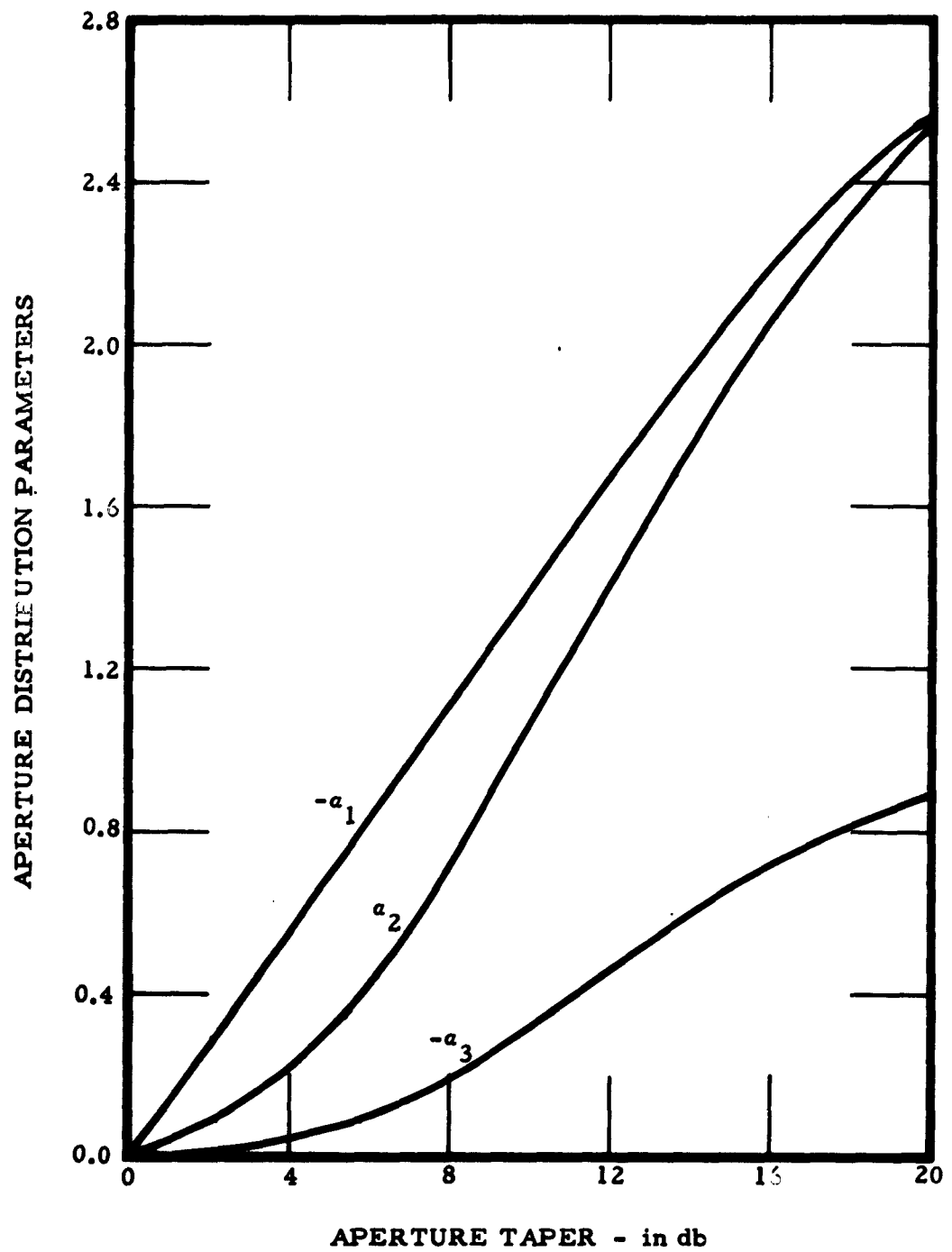


Figure 8. Aperture Distribution Parameters Versus Aperture Taper for High-Gain Paraboloidal Type Reflectors

$$F_n(\theta, R) = \text{Re}I_1 + j\text{Im}I_1 + a_1\text{Re}I_2 + ja_1\text{Im}I_2 + a_2\text{Re}I_3 + ja_2\text{Im}I_3 \\ + a_3\text{Re}I_4 + ja_3\text{Im}I_4 \quad (47)$$

where Re and Im denote the real and imaginary parts of the summation of Equation (40), and the subscripts 1, 2, 3, and 4 denote which integral of Equation (46) was used in the evaluation. This formulation has the marked advantage that once the eight field components $\text{Re}I_1$ through $\text{Im}I_4$ have been evaluated, the scalar near field of an antenna whose distribution function can be approximated by $1 + a_1\rho^2 + a_2\rho^4 + a_3\rho^6$ can be easily determined. By virtue of Equation (47), only simple operations involving additions and multiplications are required for this to be accomplished. Thus, analytical estimates of the near field behavior of reflecting-type antennas can be made by field personnel in a simple manner.

Volume II of this report contains tables of the field components of an 80λ circular aperture, for 40 values of range varying selectively between $R = 0.0125 D^2/\lambda$ and $R = 2D^2/\lambda$. The increments in range and azimuth angle are sufficiently small so that both the range and angular variations in field strength can be accurately reproduced. From these tables, the SNF of antennas of arbitrary size and aperture distribution can be computed. Included in Volume II is a complete description of the use of the tables and a number of sample problems. The interested reader is referred to Volume II for a detailed description of the SNF calculations. Justification of using calculations based upon a specific aperture size to deduce the SNF of apertures of a different size, will now be made.

4. Universal SNF Patterns

Antennas which are identical except for size, have identical far field patterns except for an angular scale factor. Advantage is often taken of this phenomenon by graphing the patterns in u space (where $u = ka \sin \theta$) in which the patterns are identical. This has the distinct advantage that one graphical representation can be used to describe the far fields of all antennas whose aperture distributions and shapes are the same.

The graphical representation of near field data cannot be accomplished as easily, however. First, since the shape of the near field patterns is dependent upon range, a family of curves is required to describe this dependence. Second, the scalar near field patterns of antennas which are identical except for size are not simply related. This implies that it is necessary to perform an independent analysis each time the antenna size is varied. The need for independent analyses greatly complicates the problem of data presentation and multiplies the cost of the computational program. For these reasons it is of importance to determine what conditions, if any, permit the prediction of the scalar near field of one antenna from that of another antenna of different size. Investigation of the small angle Fresnel approximation indicates that this is possible under restricted conditions. Within the accuracy of this approximation, the Fresnel fields of unequally-sized but otherwise identical antennas, when plotted as a function of u , are identical at distances specified by like values of $R\lambda/D^2$. Also, since the transition distance analysis indicates that at wide angles, the scalar near field tends to behave as the far field, there is reason to suspect that such predictions are possible even at wide angles.

For the case of a uniform circular aperture, the on-axis SNF integral can be evaluated in closed form. The amplitude of the on-axis field is given by

$$F_N(R, 0) = \sin \left\{ \frac{\pi}{\lambda} \left[\sqrt{R^2 + \left(\frac{D}{2}\right)^2} - R \right] \right\} \quad (48)$$

Equation (48) shows that the on-axis field of uniformly-excited circular apertures of different diameters are identical at ranges specified by like values of $\left[\sqrt{R^2 + (D/2)^2} - R \right]$. Although this is not precisely true, it is very nearly true for distributions other than uniform. Thus, in order to determine if universal SNF patterns can be constructed, from computations based upon a specific antenna size, the patterns of apertures whose diameters differ should be compared in u-space and at ranges such that $\left[\sqrt{R^2 + (D/2)^2} - R \right]$ is constant. A number of such comparisons have been made. Among others, the scalar near fields of 10λ , 20λ , 40λ , and 80λ apertures have each been compared to the SNF of an 160λ aperture at selected values of range. In each case, the range was selected to be nearly at the inner boundary of the SNF for the smaller aperture. For example, in the comparison between the 10λ and 160λ apertures, the SNF of the 10λ aperture at a range of 12λ ($R = 0.12 D^2/\lambda$) was compared to that of the 160λ aperture at a range of $3,080\lambda$ ($R = 0.1203 D^2/\lambda$). Thus, if the two scalar near field patterns were sufficiently alike, calculations on the larger aperture could be used to predict the entire SNF of the smaller aperture. Conversely, calculations on the smaller aperture can be used to predict the SNF of the larger, for ranges satisfying $R \geq D_{\max}^2/D_{\min}$.

Figures 9 through 12 show four comparisons such as described above. Figures 9 and 10 show a comparison between the scalar near

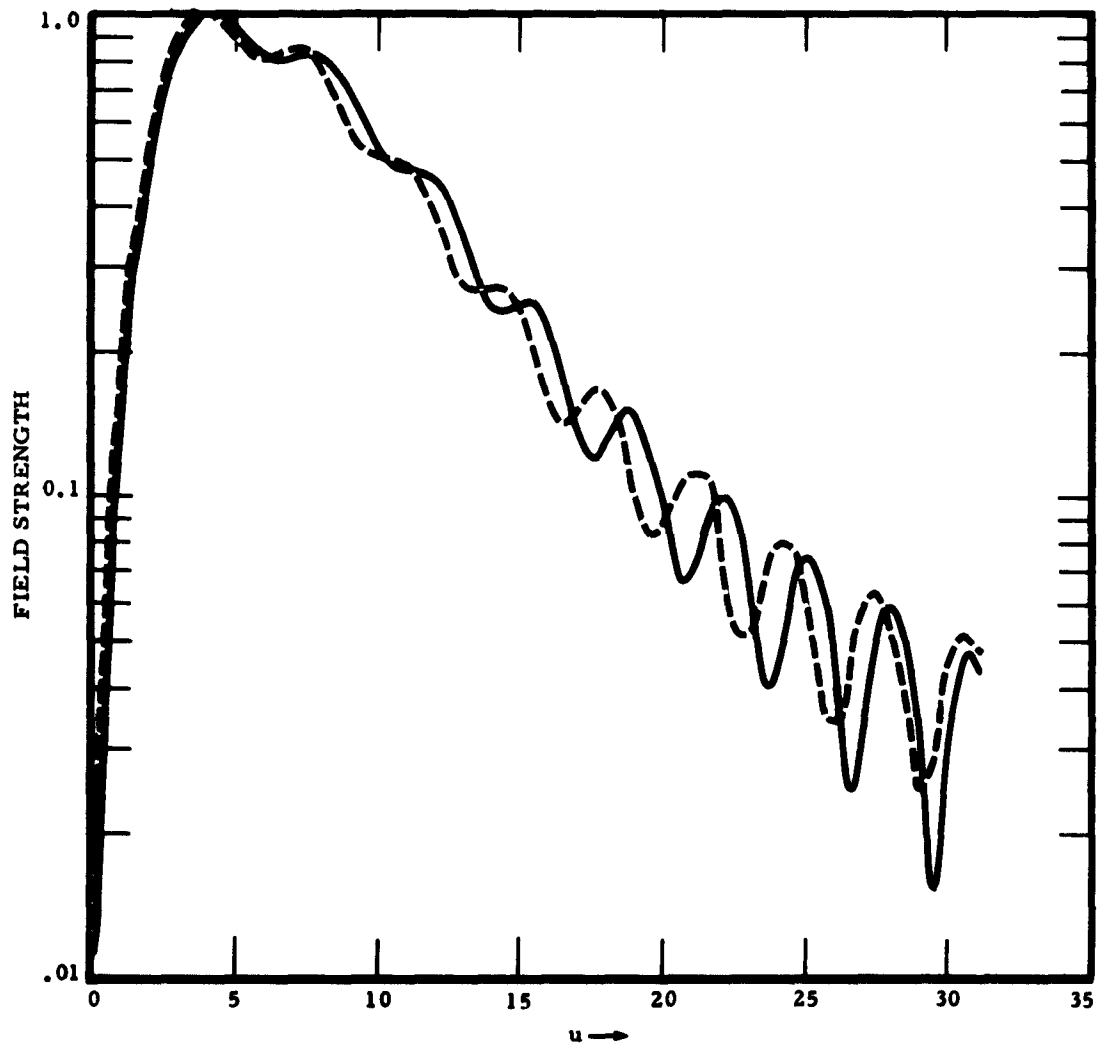


Figure 9. Comparison of the SNF of 10λ and 160λ Apertures at Approximate Range of $R = 0.12 D^2/\lambda$ - Uniform Distribution

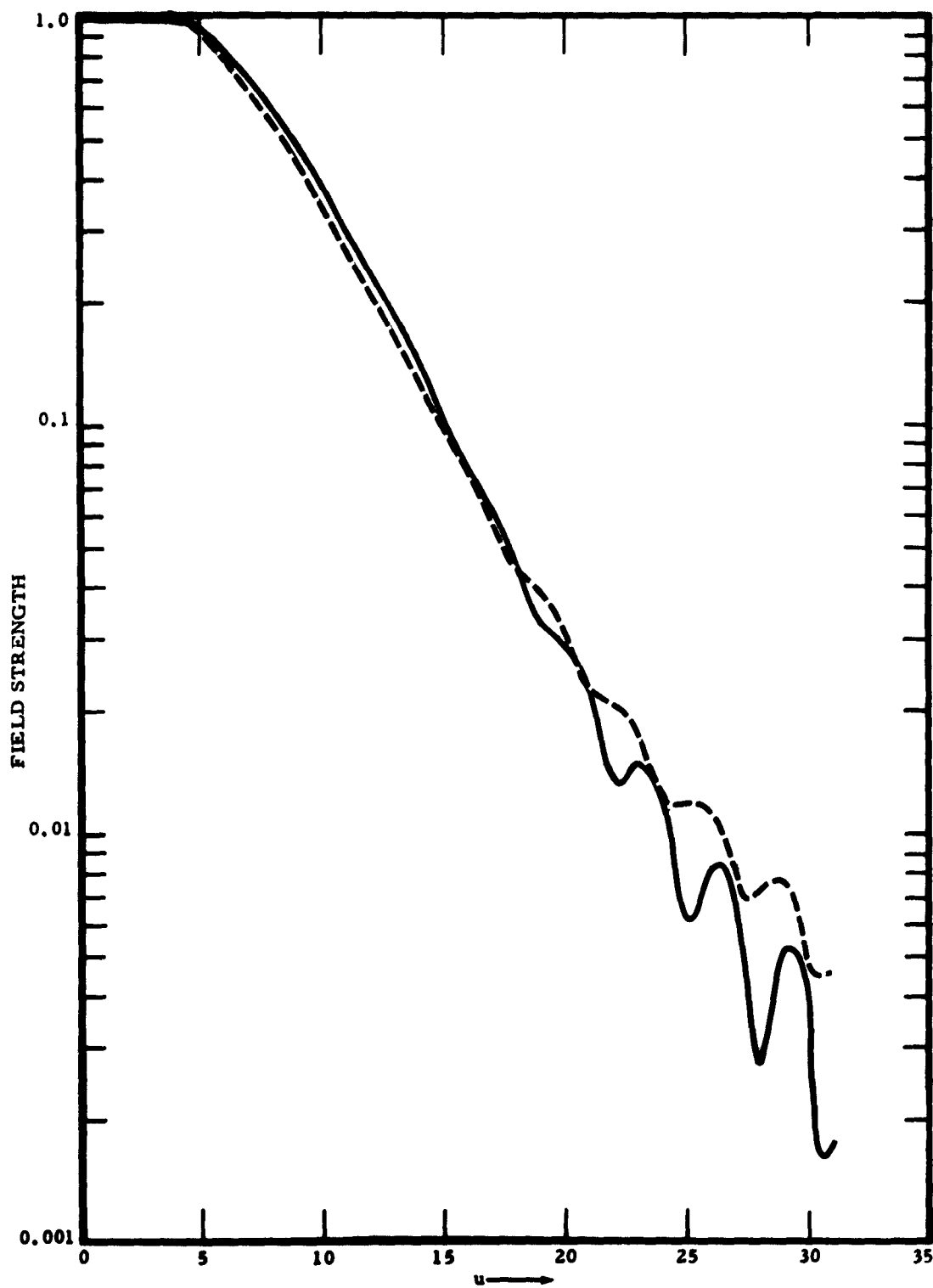


Figure 10. Comparison of the SNF of 10λ and 160λ Apertures at
 , Approximate Range of $R = 0.12 D^2/\lambda - (1 - \rho^2)$
 Distribution

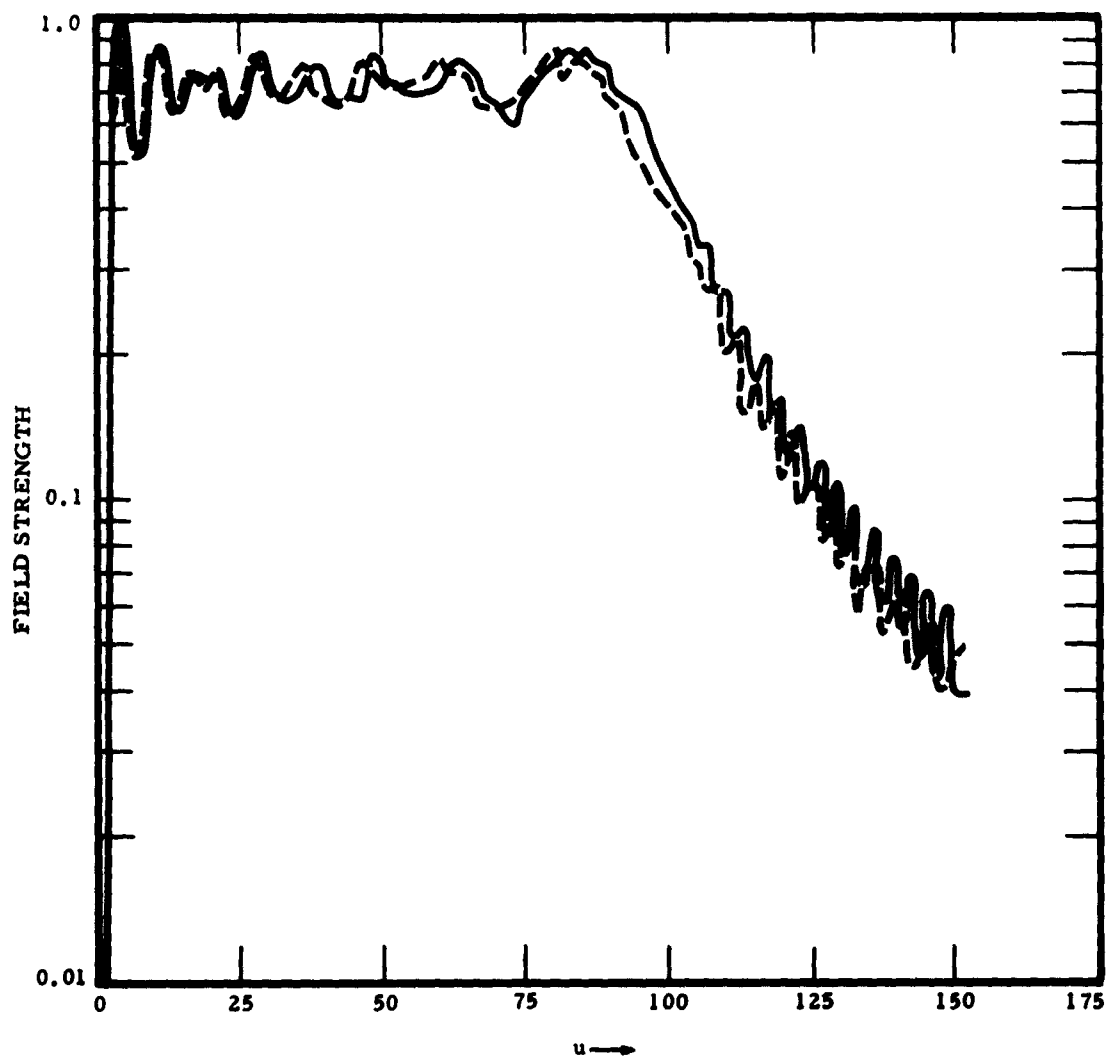


Figure 11. Comparison of the SNF of 80λ and 160λ Apertures at Approximate Range of $R = 0.015 D^2/\lambda$ - Uniform Distribution

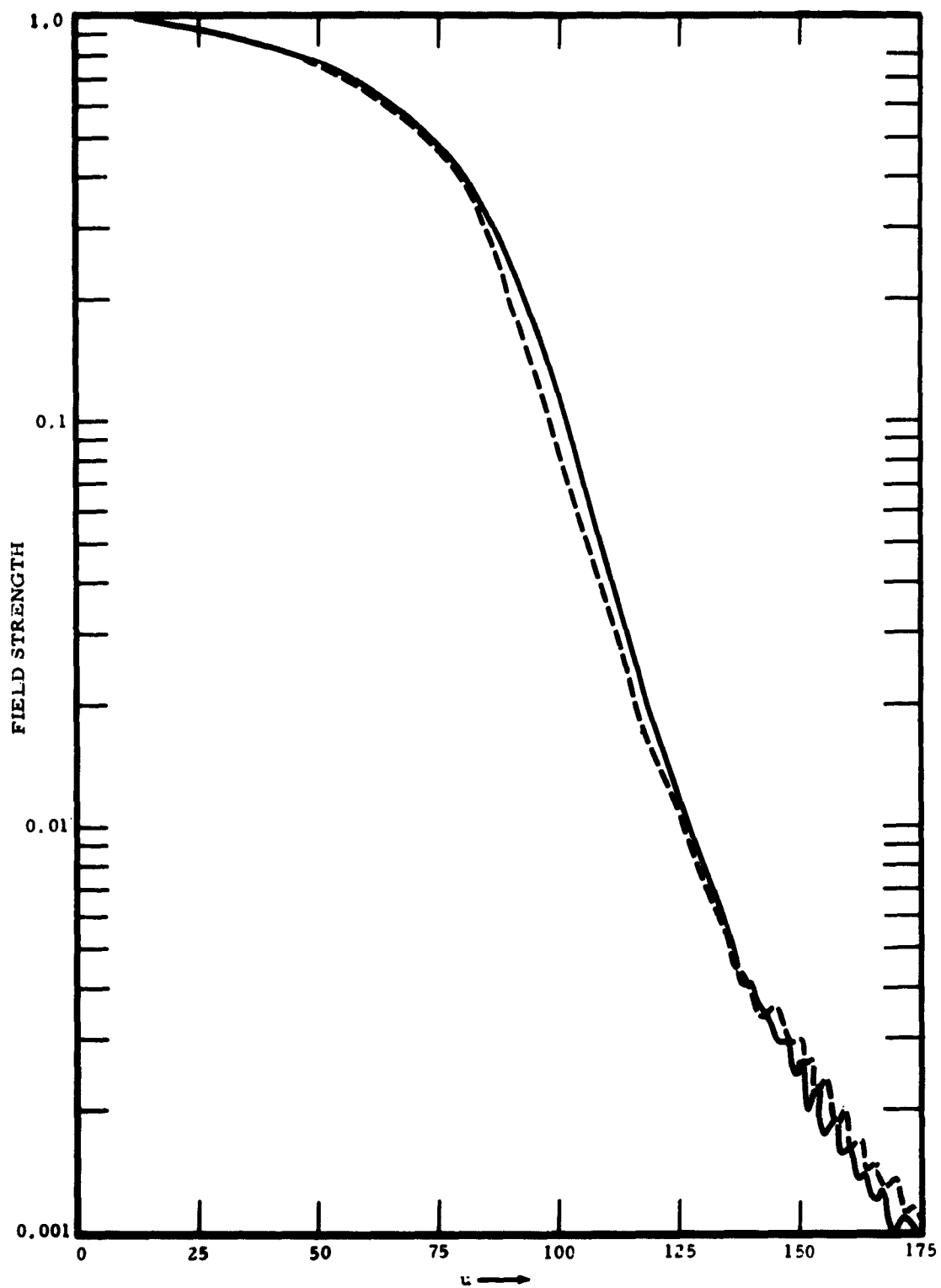


Figure 12. Comparison of the SNF of 80λ and 160λ Apertures at Approximate Range of $R = 0.015 D^2/\lambda - (1 - \rho^2)$ Distribution

fields of 10λ and 160λ apertures. In each case, the range is approximately given by $R = 0.12 D^2/\lambda$. The aperture distribution corresponding to the patterns of Figure 9 is uniform, and to the patterns of Figure 10 is $(1 - \rho^2)$. The fields are plotted against u , where $u = ka \sin \theta$. The maximum value of u considered is 10π ; for the 10λ aperture, this corresponds to an azimuthal angle of 90 degrees and for the larger aperture of only 3.58 degrees. It is seen that although the ratio of antenna sizes is 16:1, the scalar near fields of the two antennas correspond exceedingly well, even at levels as low as 40 db below the maximum.

Figures 10 and 11 compare the fields of 80λ and 160λ apertures at values of range which are approximately given by $R = 0.015 D^2/\lambda$. The aperture distribution for Figure 11 is uniform and for Figure 12 is $(1 - \rho^2)$. The fields are plotted to a value of $u = 150$, which corresponds to 36.6 degrees for the smaller aperture and 17.3 degrees for the larger. The fields were actually calculated to a value $u = 252$, which corresponds to 90 degrees for the 80λ aperture. However, the agreement between the calculations improves beyond $u = 150$, so that for convenience the graphs were terminated at this point. Again, it is seen that the differences between the fields is insignificant from a practical standpoint, although the calculations were made for a range which is quite deeply submerged in the near field.

The results of each of the comparisons made during the course of the investigation were similar to those presented herein. Thus, it can be concluded that universal SNF patterns can be constructed from calculations based upon a particular antenna size.

5. Accuracy of the Scalar Near Field Formulation

As indicated in Section III. A, the scalar near field formulation yields an approximate measure of the field strength. To gain an appreciation of the accuracy of the formulation, it is of interest to compare the results of one calculation with the exact computations of Hansen and Bailin.⁴ This is done in Figure 13, which shows a comparison of the field strengths as computed by Hansen and Bailin and by use of the scalar near field formulation for a ten-wavelength antenna at a distance of ten wavelengths. The agreement between the two curves of Figure 13 is very good to an azimuth angle of 70 degrees, beyond which no data is available on the exact field. Although this simple comparison does not definitely establish the accuracy of the scalar near field formulation, it indicates that the results of scalar near field computations can be used with assurance in the evaluation of interference phenomena.

6. On-Axis Field

The on-axis SNF is of importance in many applications, especially from the standpoint of personnel safety. Therefore, although the on-axis case can be calculated by the techniques discussed previously, it is worthy of special note. The on-axis field for the class of distributions under investigation is given by

$$F_N(R, 0) = jk \int_0^a \left[1 + a_1 \left(\frac{\rho}{a} \right)^2 + a_2 \left(\frac{\rho}{a} \right)^4 + a_3 \left(\frac{\rho}{a} \right)^6 \right] \frac{e^{-jk\sqrt{R^2 + \rho^2}}}{\sqrt{R^2 + \rho^2}} \rho d\rho \quad (49)$$

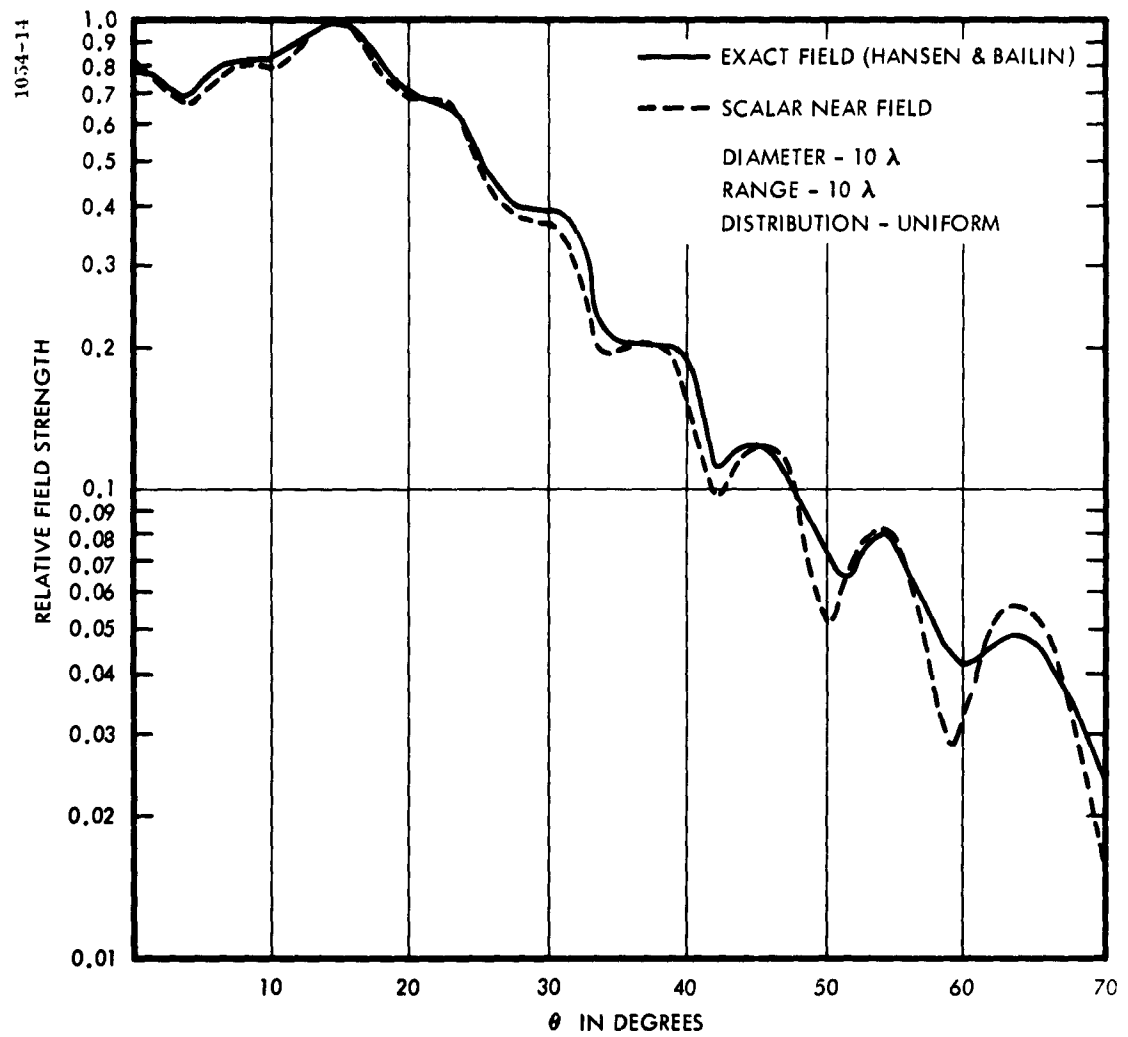


Figure 13. Comparison of Scalar Near Field Theory with Exact Theory

Equation (49) can be evaluated in closed form by noting that,

$$\frac{d}{d\rho} \left(e^{-jk\sqrt{R^2 + \rho^2}} \right) = -jk\rho \frac{e^{-jk\sqrt{R^2 + \rho^2}}}{\sqrt{R^2 + \rho^2}} \quad (50)$$

and integrating by parts. It is of interest to consider the on-axis region which is relatively close to large antennas. In this region terms of the order (λ/R) , $(\lambda/D)^2$, and $(R\lambda/D^2)$ can be ignored; and the on-axis field becomes

$$\begin{aligned} F_N(R, 0) = [f(0) + f(a)] \sin \left\{ \frac{kR}{2} \left[\sqrt{1 + \left(\frac{a}{R}\right)^2} - 1 \right] \right\} \\ + j[f(0) - f(a)] \cos \left\{ \frac{kR}{2} \left[\sqrt{1 + \left(\frac{a}{R}\right)^2} - 1 \right] \right\} \end{aligned} \quad (51)$$

where $f(0)$ is the aperture distribution at the center of the aperture and $f(a)$ is the aperture distribution at the edge of the aperture, both in volts/meter. Differentiating with respect to R , shows that the field minima occur at values of R satisfying

$$\frac{kR}{2} \left[\sqrt{1 + \left(\frac{a}{R}\right)^2} - 1 \right] = n\pi \quad , \quad n = 0, 1, 2, \dots \quad (52)$$

Similarly, the field maxima occur at

$$\frac{kR}{2} \left[\sqrt{1 + \left(\frac{a}{R}\right)^2} - 1 \right] = \frac{2n+1}{2} \pi \quad , \quad n = 0, 1, 2, \dots \quad (53)$$

Thus, the minimum and maximum field strengths are simply

$$F_N(\text{min}) = f(0) - f(a) \quad (54)$$

$$F_N(\text{max}) = f(0) + f(a) \quad (55)$$

Equations (54) and (55) are valid for values of $R\lambda/D^2 \ll 1$. Two interesting conclusions can be drawn from Equations (54) and (55). First, the maximum and minimum values of the on-axis field depend only upon the strength of the aperture distribution at the center and edge of the aperture, and are independent of the aperture diameter. Second, the ratio of the maximum to minimum on-axis field strengths depends only upon the aperture taper, and is independent of the exact shape of the aperture distribution. It is interesting to note that for a uniform distribution, the field strength varies between zero and twice the strength of the field in the plane of the aperture. However, for distributions which vanish at the edge of the aperture, the on-axis field strength (maximum and minimum) is independent of range and equals the field strength at the center of the aperture.

D. Rectangular Apertures

1. Approach

During the course of the investigation, a number of techniques for evaluating the scalar near field of rectangular apertures were discussed. Of these, the most advantageous was to analyze the principal plane patterns of rectangular apertures in terms of the scalar near field of line sources. This approach assumes that the shape of the scalar near field

in the principal planes of a rectangular aperture is determined entirely by the field distribution along the corresponding aspect of the aperture. It also assumes that, when properly modified, the product of the on-axis fields of two line sources yields the on-axis field of the rectangular aperture. These assumptions are correct to within the Fresnel approximation; it will presently be shown that the assumptions yield very good results at distances significantly less than can be justified by the Fresnel approximation.

2. Angular Variations of the SNF

In the principal plane, the scalar near field of a uniformly illuminated line source of length L , oriented in the x -direction may be written as

$$F_1(R, \theta) = \int_{-L/2}^{L/2} \frac{e^{-jk\sqrt{R^2 + x^2} - 2Rx \sin \theta}}{\sqrt{R^2 + x^2} - 2Rx \sin \theta} dx \quad (56)$$

The scalar near field in the corresponding plane of a uniformly illuminated strip aperture, of constant width L in the x -direction and infinitely long in the y -direction, is

$$F_2(R, \theta) = \int_{-L/2}^{L/2} \frac{e^{-jk\sqrt{R^2 + x^2} - 2Rx \sin \theta}}{\sqrt[4]{R^2 + x^2} - 2Rx \sin \theta} dx \quad (57)$$

as expected the line source gives rise to a set of spherical waves while the infinite strip gives rise to cylindrical waves. Thus as a function of range, the fields associated with each aperture behave quite differently. However,

the θ -dependence of the fields is strikingly similar, as evidenced by the fact that the phase terms in each integral are identical. The variation in the θ -dependence normalized to a line source field can be determined by investigating the difference

$$\left| 1 - \frac{F_2(R, \theta)}{R^{1/2} F_1(R, \theta)} \right| \quad (58)$$

which will be shown to vanish as $(L/R)^2$ for R large. By differentiating Equation (58) with respect to θ , and equating the differential to zero, it is seen that the maximum difference for finite R occurs at $\theta = \pi/2$.

Thus, to determine the maximum difference in the scalar near fields of the line source and the infinite strip apertures, only the direction $\theta = \pi/2$ need be considered. For $\theta = \pi/2$, and under the change of variables $k(R - x) = t$, Equations (56) and (57) may be written in terms of the sine- and cosine-integrals and in terms of the Fresnel integrals, respectively

$$\begin{aligned} F_1(R, \pi/2) &= - \int_{k(R + L/2)}^{k(R - L/2)} \frac{\cos t + j \sin t}{t} dt \\ &= Ci(kR - kL/2) + jSi(kR - kL/2) \\ &\quad - Ci(kR + kL/2) - jSi(kR + kL/2) \end{aligned} \quad (59)$$

and

$$\begin{aligned}
 F_2(R, \pi/2) &= \lambda^{1/2} \frac{1}{2} \int_{k(R - L/2)}^{k(R + L/2)} [J_{-1/2}(t) + jJ_{1/2}(t)] dt \\
 &= \lambda^{1/2} [C(kR + kL/2) + jS(kR + kL/2) \\
 &\quad - C(kR - kL/2) - jS(kR - kL/2)] \quad (60)
 \end{aligned}$$

Under the conditions $R \geq L$, $L/\lambda \geq 10$, the asymptotic representations for the sine- and cosine-integrals and for the Fresnel integrals may be used with negligible error. The asymptotic limits for the Fresnel integral are given in Equation (28); asymptotically, the sine- and cosine-integrals approach

$$Ci(x) + jSi(x) \approx \frac{e^{jx}}{jx} \quad (61)$$

selecting the aperture width, L , to be an odd number of half wavelengths, which makes $\theta = \pi/2$ correspond with the direction of a far field sidelobe, and using the asymptotic limits for the functions of Equations (59) and (60), Equation (58) becomes

$$\begin{aligned}
 \left| 1 - \frac{F_2(R, \pi/2)}{R^{1/2} F_1(R, \pi/2)} \right| &= 1 - \frac{R^2 - (L/2)^2}{2R^2} \left(\frac{1}{\sqrt{1 - L/2R}} + \frac{1}{\sqrt{1 + L/2R}} \right) \\
 &\approx 0.156(L/R)^2 \quad (62)
 \end{aligned}$$

For the minimum range of interest, $R = L$, the normalized difference between the two patterns is approximately 0.156. This means that in directions corresponding to the far field maxima the greatest difference between the normalized patterns of the line source and infinite strip apertures is approximately 1.5 db. If the range is increased to a value of $2L$, the difference between the patterns diminishes to approximately 0.3 db. Thus, in the principal plane, the angular dependence of the line source pattern is essentially identical to that of the infinite strip aperture even at very short ranges.

To conclude the argument that the shape of the scalar near field in the principal plane of a rectangular aperture is determined almost entirely by the field distribution along the corresponding aspect of the aperture, an aperture which is finite in both dimensions will be considered. The distribution function will be selected to be uniform in the x -direction and gabled in the y -direction. For convenience the aperture will be taken to be square, of length L on a side. The field will be calculated at a range $R = L$, in the principal plane which is orthogonal to the x -axis. It will be shown that even at this close range the field is but slightly different from that of the infinite strip aperture.

The scalar near field in the principal plane of interest is given by

$$F(R, \theta) = 2 \int_{-L/2}^{L/2} dx \int_0^{L/2} \left(1 - \frac{2y}{L}\right) \frac{e^{-jk\sqrt{w^2 + y^2}}}{\sqrt{w^2 + y^2}} dy \quad (63)$$

where $w^2 = R^2 + x^2 - 2Rx \sin \theta$. The y-integral can be extracted by partial integration, which yields for the SNF:

$$F(R, \theta) = j \int_{-L/2}^{L/2} \left[\pi H_0^{(2)}(kw) - \frac{2e^{-jkw}}{kL/2} \right] dx \quad (64)$$

using the asymptotic representation for the Hankel function, Equation (64) becomes

$$F(R, \theta) = j \int_{-L/2}^{L/2} e^{-jkw} \left(\sqrt{\frac{\lambda}{w}} - \frac{2\lambda}{\pi L} \right) dx \quad (65)$$

From Equation (65) it is clear that under the condition that $\left(\frac{\lambda}{w}\right)^{1/2} \gg \frac{2\lambda}{\pi L}$, the scalar near field of the finite aperture is negligibly different from that of the infinite strip aperture. This is satisfied if w is of the order of L and if $L \gg \lambda$, which are precisely the conditions of interest.

From the above analysis it can be concluded that in the principal plane the scalar near field of a rectangular aperture is negligibly different in shape from that of a line source with a corresponding length and aperture distribution. Thus, the rectangular aperture analysis is reduced to the analysis of a line source with respect to obtaining the θ -variations of field in the principal planes.

3. Range Variations of the SNF

Line source theory, also permits an approximate determination of the range dependence of rectangular apertures. When properly modified, the product of the on-axis fields of two line sources closely approximates the on-axis field of a rectangular aperture. Since the angular variations have been obtained previously, this is all that is required for a total solution.

The on-axis SNF integral for a rectangular aperture of dimensions L_1 and L_2 is

$$F_N(R, \theta) = \int_{-L_1/2}^{L_1/2} \int_{-L_2/2}^{L_2/2} f(x) f(y) \frac{e^{-jk\sqrt{R^2 + x^2 + y^2}}}{\sqrt{R^2 + x^2 + y^2}} \quad (66)$$

In the investigation, the following approximation was made for the SNF integral

$$F_N(R, \theta) = R e^{jkR} \int_{-L_1/2}^{L_1/2} f(y) \frac{e^{-jk\sqrt{R^2 + y^2}}}{\sqrt{R^2 + y^2}} dy \int_{-L_2/2}^{L_2/2} f(x) \frac{e^{-jk\sqrt{R^2 + x^2}}}{\sqrt{R^2 + x^2}} dx \quad (67)$$

In the development of Equation (67), the following approximations were used,

$$\left(R^2 + x^2 + y^2\right)^{1/2} = \left(R^2 + x^2\right)^{1/2} + \left(R^2 + y^2\right)^{1/2} - R \quad (68)$$

in the phase term, and

$$\left(R^2 + x^2 + y^2\right)^{1/2} = R^{-1} \left(R^2 + x^2\right)^{1/2} \left(R^2 + y^2\right)^{1/2} \quad (69)$$

in the amplitude term. By expanding each of the terms in Equations (68) and (69) in a binomial series, both of the approximations are seen to be significantly better than the Fresnel approximations. The approximations are poorest for a square aperture, and improve rapidly as the aperture's aspect ratio increases. For all ranges and antenna sizes of interest, the approximation for the amplitude term introduces negligible error, even for the square aperture case.

As can be seen from Equation (68), the "phase error" introduced by the approximation for the phase term vanishes along the principal aspects ($x = 0$ or $y = 0$) of the aperture. The "phase error" is greatest along the diagonals and attains its maximum value at the corners of the rectangular aperture. The "phase error" is proportional to L_1/λ , and is shown in Figure 14 as a function of R/L_1 , for various values of L_1/L_2 . From Figure 14, it is seen that for a square aperture 100 wavelengths on a side, the "phase error" at $R = 100\lambda$ is about 410 degrees. However, for an aperture $100\lambda \times 50\lambda$, the "phase error" at $R = 100\lambda$ is only about 11.5 degrees. For the square aperture case, the error introduced by the approximation of Equation (68) decreases very rapidly with increasing range; at $R = 2L_1$, the error is only about 65 degrees for the 100λ aperture, and 19 degrees at $R = 3L_1$. Thus, except for large square apertures and ranges in the immediate vicinity of $R = L_1$, the line source approach yields excellent results with respect to predicting the SNF of rectangular apertures. Even for the square aperture case, it is doubtful

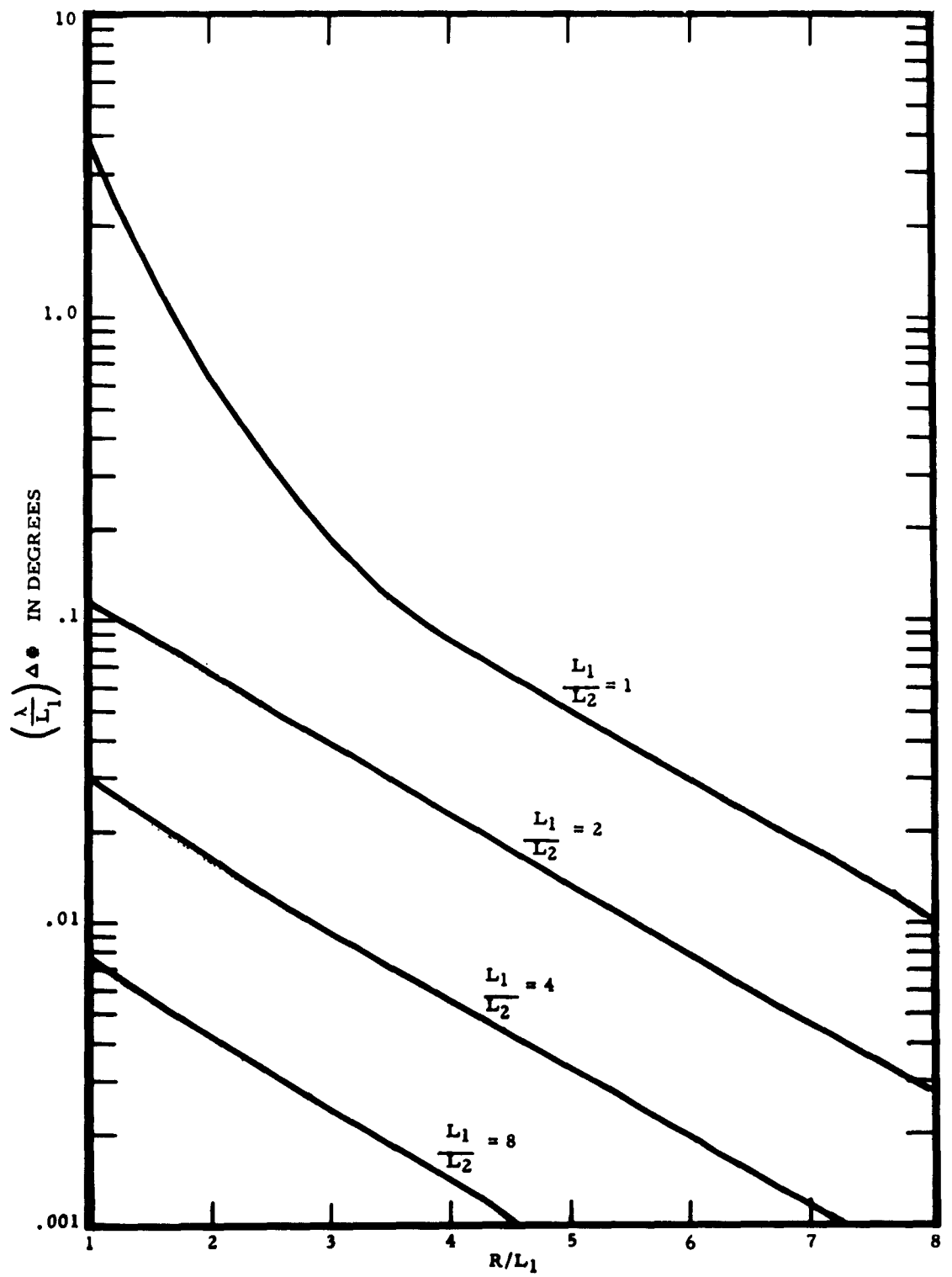


Figure 14. Maximum Phase Error in Rectangular Aperture Versus Range

that the calculations will be more than a few db in error, due to the fact that the phase errors are highly localized, and because their effect is minimized by integration.

4. Mathematical Formulation

By using the addition theorems for the spherical Bessel functions and the Legendre polynomials in a similar manner as was done for the circular aperture case, the SNF of a line source may be written,

$$F(R, \theta) = \left(\frac{1 + \cos \theta}{2} \right) \sum_{n=0}^{\infty} (2n + 1) P_n(\sin \theta) h_n^{(2)}(kR) \int_{-L/2}^{L/2} f(x) j_n(kx) dx \quad (70)$$

The line source formulation of Equation (70) is nearly identical to the formulation of Equation (40) used in the circular aperture case. This has allowed a single computer program to be written which can be used for both cases, and has resulted in a significant saving in time, effort, and expense.

5. Evaluation of the SNF

From this point, the procedure used to determine the SNF of rectangular apertures is almost identical to that used for circular apertures. Volume II of this report contains extensive SNF tables for line sources, from which the SNF of rectangular apertures whose size, aspect ratio, and aperture distribution function are arbitrary, can be constructed. These calculations were based upon an aperture length of 80λ , but are valid for a wide range of antenna lengths. This has been established by comparisons which are identical to those reported for the circular aperture case. The results of the comparisons for the two cases are virtually identical.

For rectangular apertures of dimension L_1 and L_2 , the aperture distribution function is selected as

$$f(x, y) = \left[1 + a_1 \left(\frac{2x}{L_1} \right)^2 + a_2 \left(\frac{2x}{L_1} \right)^4 + a_3 \left(\frac{2x}{L_1} \right)^6 \right] \left[1 + a'_1 \left(\frac{2y}{L_2} \right)^2 + a'_2 \left(\frac{2y}{L_2} \right)^4 + a'_3 \left(\frac{2y}{L_2} \right)^6 \right] \quad (71)$$

unlike the circular case, a universal set of the aperture distribution parameters, a_n, a'_n , is not meaningful, because a variety of distributions is commonly used with rectangular apertures. Fortunately, however, rectangular antennas are usually designed on the basis of the aperture distribution, and it is known in most cases. Thus, the aperture distribution parameters can usually be obtained by curve fitting.

A complete explanation of the SNF calculation for rectangular apertures is given in Volume II, to which the interested reader is referred.

E. Additional Considerations

The preceding analyses were conducted on the basis of a free-space environment and operation at the design frequency. Thus, such factors as feed spillover, leakage through mesh-type reflectors, ground reflections, and spurious radiations have been neglected. Presumably, the above factors can significantly affect the intrasite interference picture. Unfortunately, however, analytical techniques are found wanting from the standpoint of determining these effects in a general fashion. For example, spurious radiations depend not only on the type of antenna, but on its age and condition, the type of power tube, and the operating power level. The picture is even more complicated with respect to site reflections.

Additionally, an "optimum" analytical approach depends on the manner in which the results of the analysis are to be used. For example, if the prime purpose of the analysis is to determine the probability of interference in a general situation, the uncertainties introduced by the above factors can be related to the standard deviation of a statistic which describes the spatial distribution of energy associated with antennas. Thus, a detailed description of the spatial distribution of energy in the presence of the disrupting factors, would not be required. However, if the purpose of the analysis is to isolate the exact causes of interference in a specific situation, a more detailed analysis is needed.

For these reasons, the effort extended into the above areas was very limited, and few definitive results were obtained. Thus, the present discussion is limited to general observations with respect to the importance of these factors to the total RFI picture.

The problem of transmission through meshes is of interest in an RFI investigation because many reflector-type antennas are made of grids or meshes through which part of the energy may be propagated. Thus, the energy density in the "shadow" region will depend on the transmission characteristics of the gratings used in the reflector's construction.

The problem of transmission through gratings has been studied both theoretically and experimentally by several investigators over a number of years. Notable among these investigators have been Hayes,¹⁰ Wilson and Cottony,¹¹ Groves,¹² and Mumford.¹³ Their work has been reviewed by ASI and found to be in good agreement and the results of these investigations can be used to estimate the energy density in the shadow region for common antenna types.

These investigations indicate that even at the design frequency the leakage fields can be appreciable. Depending on the design of the grid structure, the power leakage can vary between about one-tenth of one percent and three percent. At spurious frequencies, the percentage of power in the leakage field increases rapidly and can reach values of fifty percent or more.

Feed spillover can also have significant effects. The amount of spillover varies with the aperture taper and type of feed. For example, with a cassegranian feed it is possible to design an almost uniformly illuminated antenna with very little spillover. With conventional feeds this is not generally the case. The amount of power in the spillover field is often as great as five percent of the total radiated power.

Since the presence of reflected waves can appreciably alter the distribution of energy in the near zone, the implications of ground reflections with respect to RFI are apparent. The magnitude of the reflections depends upon many factors, including: the presence or absence of architectural structures and vegetation, ground conductivity, the operating polarization, the ground roughness, and the extent of smooth ground. Each of these factors varies between sites and is affected by such factors as the weather and seasonal changes. Therefore, the task of constructing a meaningful mathematical model that accurately accounts for site reflections is extremely difficult, if not impossible. Thus, simplifying approximations must be made in the theoretical approach to the site reflection problem.

The simplest approach towards estimating the effect of the ground is to assume that it behaves as a smooth conductor of infinite extent. Under such an assumption, the total fields can be calculated by image theory.

Even such a simplified approach results in a mathematically complicated problem. This is due to the fact that in order to obtain the total near field, the scalar near fields of two antennas (the real and the image antenna), must be added. In performing the addition, the fields emanating from each must be written with respect to a common coordinate frame. Since in the present study the calculations have been performed about a coordinate frame whose origin is at the center of the actual antenna, a linear transformation of coordinates is required to express the fields of the real and image antennas in a common frame. Although such a transformation is straightforward, the field expressions become very cumbersome and the calculation of the total field becomes tedious and costly. When it is recalled that the assumption of a perfect ground plane is highly idealized and that this assumption yields at best gross approximations to the actual fields, the advisability of performing detailed and rigorous analyses is questionable. A less rigorous analysis can be performed with considerable facility, however. The basis of this analysis is to use the far field of the image antenna to estimate the reflected field in the near region. This approach is justified when the wide angle lobes of the image antenna's radiation pattern are the primary contributors to the reflected field in the near zone, because at wide angles the scalar near field tends to follow the Fraunhofer field. Because of the gross approximations inherent in this approach it cannot be relied upon to predict the detailed structure of the near field. However, it does allow an estimate to be made of the relative importance of the reflected field, especially with respect to the generation of localized areas of high field. This latter problem is of particular importance with respect to RFI applications.

The magnitude of the disturbance at a given point depends, of course, on the relative intensities of the direct and reflected signals at that point and the phase with which these signals add. The signal intensities, in

turn, depend on the angles subtended by the field point and the electrical axes of the real and image antennas. Generally as the angles increase, the field intensities decrease although not monotonically because of the lobed structure of the fields. The phase with which the fields add depend on the height of the real antenna above the ground and the position of the field point.

A simple example, in which the transmitting antenna is directed at the horizon, is helpful in visualizing the effect of ground reflections. The exact phase with which the direct and reflected signals add will be neglected. This procedure is justified because the maximum effects occur when the signals add either in-phase or out-of-phase. For points on the ground, the angles subtended by the axes of the real and image antennas are equal; thus the intensities of the direct and reflected signals are equal. For points above the ground the angle subtended by the axis of the real antenna decreases and the angle subtended by the axis of the image antenna increases. Thus the effect of the reflected field will diminish as the observation point is raised above the ground. However, as the field point approaches the zenith, the difference between the angles approaches zero. Therefore, if the elevation of the field point continues to increase, the relative importance of the reflected wave will eventually increase.

It can therefore be concluded that the maximum disturbances are likely to occur in the directions of the horizon and of the zenith. In these directions, the signal intensity can be as much as six decibels above that calculated on the basis of free space operation if the direct and reflected fields add in phase. If the signals add out of phase, the field can vanish in these directions. In actual operation, the maximum increase or decrease in signal level would be less pronounced due to the effects of ground absorption and nonspectral scattering.

Predicting the antenna's behavior at nondesign frequencies rests upon the ability to predict the antenna's aperture distribution and efficiency at these frequencies. If the aperture distribution is known, the scalar near field can be determined by the techniques developed in the present study program. However, it is theoretically possible to determine the aperture distribution only if the geometry of the antenna circuitry is completely specified. Even for relatively simple feed geometries, the problem is very complex due to such factors as the generation of higher-order modes. In complicated feed structures, such as are common to array-type antennas, the difficulties increase by orders of magnitude. However, for illustrative purposes, it is of interest to consider the far field behavior of a horn-fed reflector type antenna with regard to harmonic operation. Consideration of the far field serves to delineate those facets of the problem which arise because of operation at nondesign frequencies. Extension of the results to the near field can be accomplished as indicated previously.

Neglecting phase-error effects in the primary feed and the possible existence of high-order modes, the illuminating pattern is dictated solely by the horn size in terms of wavelengths. Proceeding, consider the illumination pattern at the fundamental frequency to result in a highly tapered aperture distribution function. This results in a far field pattern with low sidelobes and typifies an operational radar system. Increasing the frequency has the effect of narrowing the illuminating beam, increasing the taper of the aperture illumination function, and results in further decreasing the sidelobe level. The trend would continue as long as the illumination remains a constant-phase distribution and reaches its limit when the taper becomes zero at the aperture edge. This would occur when the first null angle of the primary feed is coincident with the angle subtended by the

reflector-feed assembly which, for typical antennas, is perhaps fifty percent above the design frequency. If the operating frequency continues to increase beyond this condition, the reflector will then be illuminated by secondary lobe energy of the feed pattern in addition to its main lobe. This introduces out-of-phase illumination at the periphery of the aperture which raises the sidelobes and can eventually result in bifurcation of the main beam. Total splitting of the main beam will occur at approximately twice the design frequency. As the frequency increases further, the generation of multilobed patterns occurs.

The above discussion illustrates the type of behavior that can be anticipated by operation at other than the design frequency. However, several factors which influence the frequency response have not been accounted for. The foremost is the possibility of higher order modes which can distort the primary feed pattern and thus, the illumination of the reflector. To theoretically estimate the primary feed pattern, it is necessary to know the modal content of the fields in the mouth of the primary feed horn. Next, the wavefront in the antenna feed has been assumed to be planar at all frequencies. Actually, the wavefront is curved; the amount and type of curvature depends upon the feed horn's geometry. For instance, the wavefront is cylindrical for the sectoral horn. This deviation from the planar wavefront introduces a phase error across the primary feed aperture. In practice, a tolerable phase error is allowed at the design frequency and is adjusted to be a sufficiently small fraction of a wavelength. This results in a nearly constant phase distribution over the aperture. Since the phase error increases proportionally with frequency, the distortion of the phase front from a plane can be significant at nondesign frequencies. This is characterized by reduction in on-axis gain and higher sidelobe levels in the primary feed pattern.

Additionally, two other factors influence the frequency response of reflector-type antennas: mechanical tolerances and the location of the feed horn's center-of-phase. It is apparent that minor deviations in the shape of the reflector from a paraboloid will affect the secondary pattern increasingly as the frequency increases. Also, as the frequency varies over several octaves, the location of the center-of-phase of the primary feed can vary significantly. This defocuses the secondary patterns. The effect of each of these factors is to destroy the sharp character of the secondary pattern by filling in the nulls. Thus, in practice, the main lobe bifurcation and subsequent generation of multilobed patterns due to the increase in frequency will be moderated by the phase error effects.

F. Pattern Measurement

Although not directly related to RFI, the problem of measuring far field patterns in the near fields of large antennas is becoming of increasing interest.

One of the more promising approaches to this problem is the possibility of focusing the antenna at some distance compatible with available pattern ranges and measuring equipment. R. W. Bickmore¹⁴ has accomplished this with linear arrays by physically curving the antenna so that the resulting wave shape converges spherically. Unfortunately, in the case of reflector-type antennas, this technique is highly impractical. On-axis shifting of the feed has been investigated for such antennas, with some success; however, this is at best an approximate solution and is limited by aberration effects and the physical difficulty of shifting the feed.

ASI's interest in this problem has led to a number of measuring techniques, two of which have been reported in the literature.^{15, 16} The present discussion is concerned with an investigation of focusing by means of a lens placed between the feed and the reflector. Basically, this analysis consists of illuminating a parabolic dish with a point source placed at a finite nonfar field distance on the axis of the reflector. The reflected wave passes through a lens which focuses it on the antenna feed. By virtue of the reciprocity of geometrical optics, the lens surface computed from this analysis will transform a spherical wave, emanating from the feed, into an incident wavefront which, when reflected by the dish, will converge to the position of the original illuminating point source. Thus, the antenna will be focused at this point.

The first step in this procedure is to analyze the wavefront produced by a parabolic reflector which is illuminated by a spherical rather than a planar wavefront. The approach of Kelleher¹⁷ is suitable for this. This approach has derived a vector expression relating an incident wavefront, a reflector, and reflected wavefront, such that given any two, the third may be determined.

After the reflected wavefront has been computed, the remaining step is to determine the shape of a lens, which will convert this wavefront into a spherical wave, centered at the feed point of the reflector. To accomplish this, it has been necessary to derive an expression relating a general incident wavefront, a lens surface, and the refracted wave. This has been done by following a procedure similar to Kelleher's reflector analysis.

Using these concepts, an example has been worked out in which a parabolic dish antenna, $\left(\frac{f}{D} \text{ ratio of } 0.5\right)$ has been focused at a distance of

five diameters from the vertex of the parabola. The analysis determined a suitable family of single surface lenses of relative dielectric constant $\epsilon = 2$. Figure 15 shows a cross-section of the reflector and two of the possible lenses. Also shown are typical traces of rays emerging from a finite point on the axis. The corresponding rays emerging from infinity and being reflected on the focus (in the absence of the lenses) are also shown.

It is seen from Figure 15 that the rays which come from a finite point and from infinity converge on the focus of the parabola from different directions. If the aperture distribution is to be the same in the presence and the absence of the lenses, the rays should converge at the same angle. Thus, the single surface lenses will appreciably distort the aperture distribution and, consequently, the pattern measurement will be in error. Thus, it has been concluded that a single-surface lens is incapable of providing the proper focusing for far field measurement in the near zone.

This difficulty can be overcome by designing a double surface lens, in which the additional degree of freedom permits the aperture distribution to be unaltered. Basically, the design of the double surface lens is an extension of the design of the single surface lens.

G. Experimental Program

1. Test Apparatus

The experimental program consisted of measuring the on-axis power density of three X-band antennas; a parabolic dish antenna, a slotted rectangular waveguide array, and a slotted radial waveguide array. The test setup is pictured in Figure 16, which shows the dish antenna in

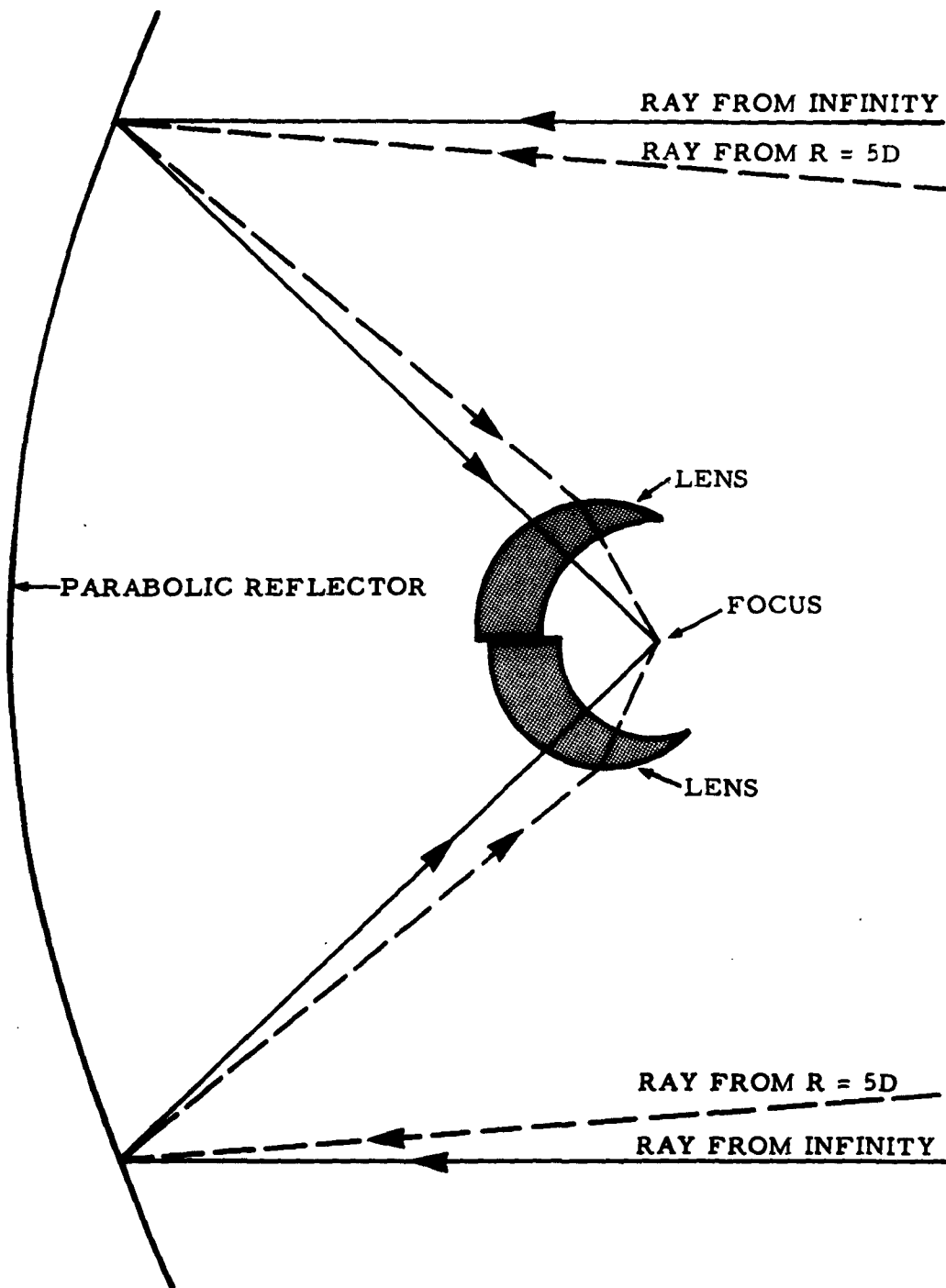


Figure 15. Single-Surface Lens for Antenna Focusing

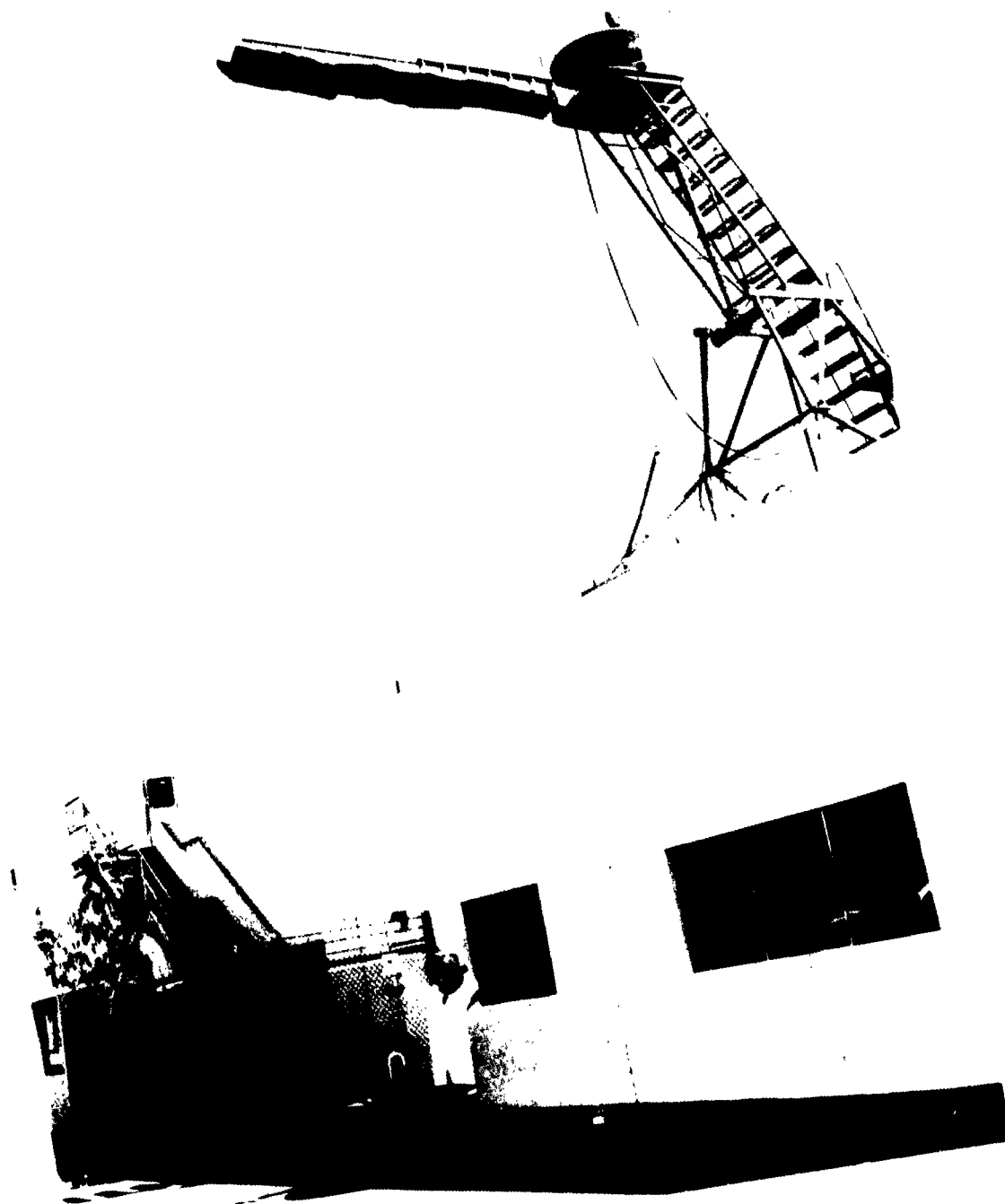


Figure 16. On-Axis Field Measuring Setup

proper test position. As can be seen, the test antenna radiates vertically upward, minimizing site reflections; the test probe, which is simply an open-ended rectangular waveguide, is raised automatically along the bore-sight axis. This is accomplished by means of a cable attached at one end to the probe and at the other to a four-foot plywood disc which is fastened to the turntable of an azimuthal antenna mount. The cable that carries the audio output signal was used for this purpose. When the mount is energized, the cable raps around the plywood disc, raising the pickup probe. By synchronizing the chart drive of a pattern recorder with the orientation of the pattern mount, a continuous plot of the on-axis power is obtained in exactly the same fashion as a radiation pattern is commonly obtained.

As can be seen from Figure 16, the test antenna is placed at ground level, approximately 12 feet from the side of the ASI building, and the azimuthal antenna mount is positioned on top of an aerostand which is on the roof of the ASI building. In this way, the field can be probed to a distance approximately 30 feet from the plane of the aperture. The test probe is restricted from rotating and kept on the boresight axis by the use of three nylon guide lines, which are fixed at the test antenna and to a ladder that projects horizontally from the aerostand. The underside of the ladder is covered with hairflex absorber to minimize reflections.

The test setup described above worked extremely well in still air. However, even a moderate breeze would cause the test probe to oscillate, degrading the accuracy of the results. Therefore, all measurements were made under calm conditions. In calm air, a run could be made in a matter of seconds; this eliminated problems due to transmitter instability, allowed the repeatability of the test setup to be easily ascertained by multiple runs, and facilitated the problem of making runs at several frequencies.

Additionally, the existence of a continuous plot of on-axis power density versus distance insured that the character of the on-axis field was faithfully reproduced, and allowed the effect of reflections from the test probe and its holding fixture to be ascertained.

A typical on-axis power density run is shown in Figure 17. This run was made for a circular planar array made of five concentric rings of crossed slots cut in a radial waveguide. (This antenna is discussed in more detail in Section III, G. 4.) Probe reflections are evidenced in this curve by the presence of a high frequency ripple. Inspection shows that the separation between ripples is almost precisely one-half wavelength, as is expected. Although the ripple has significant amplitude (as much as one decibel for ranges greater than 10λ), the effect of the ripple is easily eliminated by averaging the maximum and minimum values. Thus, the inaccuracies introduced by probe reflections probably do not exceed ± 0.1 db with the test setup employed. Such accuracy could not be obtained by probing the on-axis field at discrete points.

2. Parabolic Reflector

The parabolic reflector used in the current investigation is shown in Figure 18. This figure also shows the pick-up probe, holding fixture, and the nylon guide lines employed in the test setup. The parabola is a four-foot Andrews dish, model number D4, and the feed is an Andrews X-band button hook model number F4-71G. The E- and H-plane aperture distributions, as deduced from primary feed pattern measurements, are shown in Figure 19. The measurements were made at a frequency of 9.8 Gc for which the dish diameter is 40λ . It is worthy of note that the measured distributions are highly tapered, the current at the edge of the aperture being

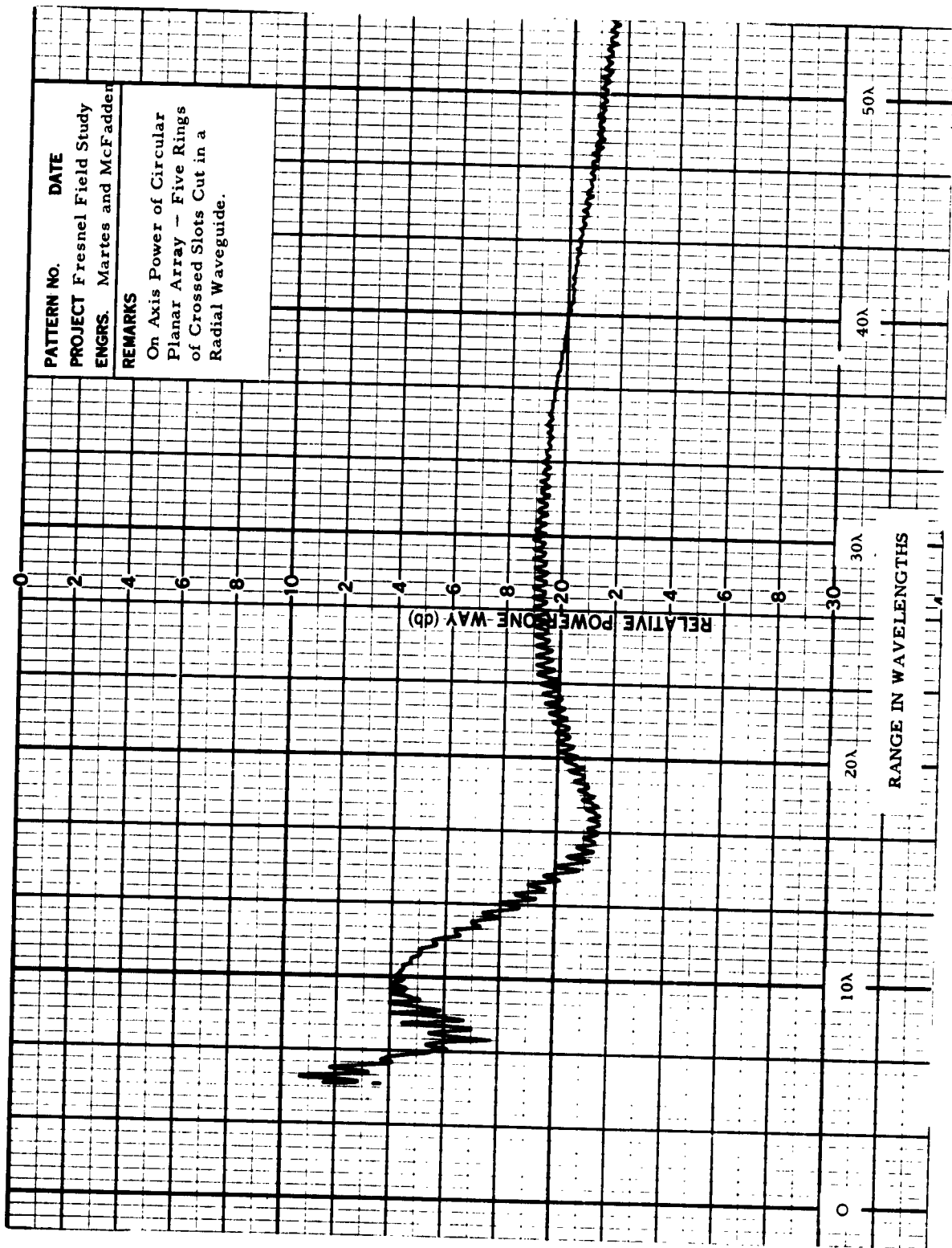


Figure 17. On-Axis Power Measurement - Sample Data



Figure 18. Four-Foot X-Band Parabolic Dish

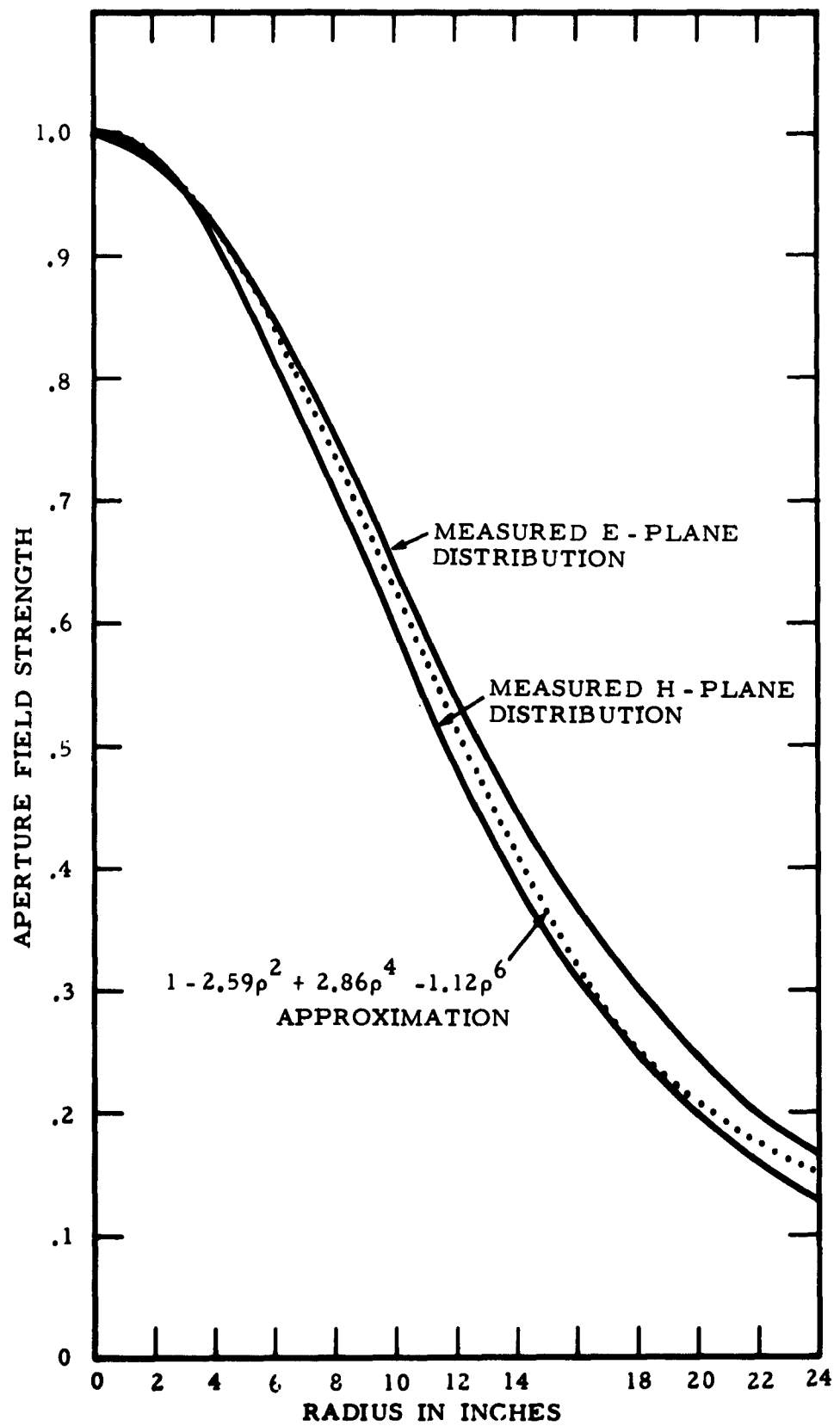


Figure 19. Aperture Field of Four-Foot Parabolic Dish

16 to 17 db below that at the center of the aperture. The measurements indicate that, except for the asymmetries introduced by the presence of the primary feed, the aperture distribution is very nearly circularly symmetric.

The theoretical and experimental curves of the on-axis field distribution associated with the 40λ dish antenna are shown in Figure 20. It is seen that the curves agree reasonably well, except for the ratio of the maxima to minima values in the region $R/D < 3.5$. The maxima are approximately 2.5 db above the minima in the theoretical curve and less than 1 db above the minima in the measured curve. However, the positions of the maxima and minima agree quite closely as do the relative behavior of the on-axis field distributions for $R/D > 3.5$.

3. Linear Array

To verify the line source computations, the on-axis field of a linear array was measured and compared with the theoretical distribution as computed by Equation (70), in which θ is set equal to zero. The array is made of 40 longitudinal slots cut in the broad-wall of a rectangular waveguide, and is pictured in Figure 21. The array is of the standing-wave type and was designed for a uniform amplitude distribution. When tested, it was placed in a ground plane whose dimensions are 25 by 39 inches. The theoretical and experimental curves are shown in Figure 22. Agreement between theory and experiment is very good except for a slight discrepancy in the positions of the relative maxima and minima. The agreement is particularly good in light of the fact that the theoretical curve is based on a continuously-excited line source and the measurements were made on a line source of discretely spaced elements.

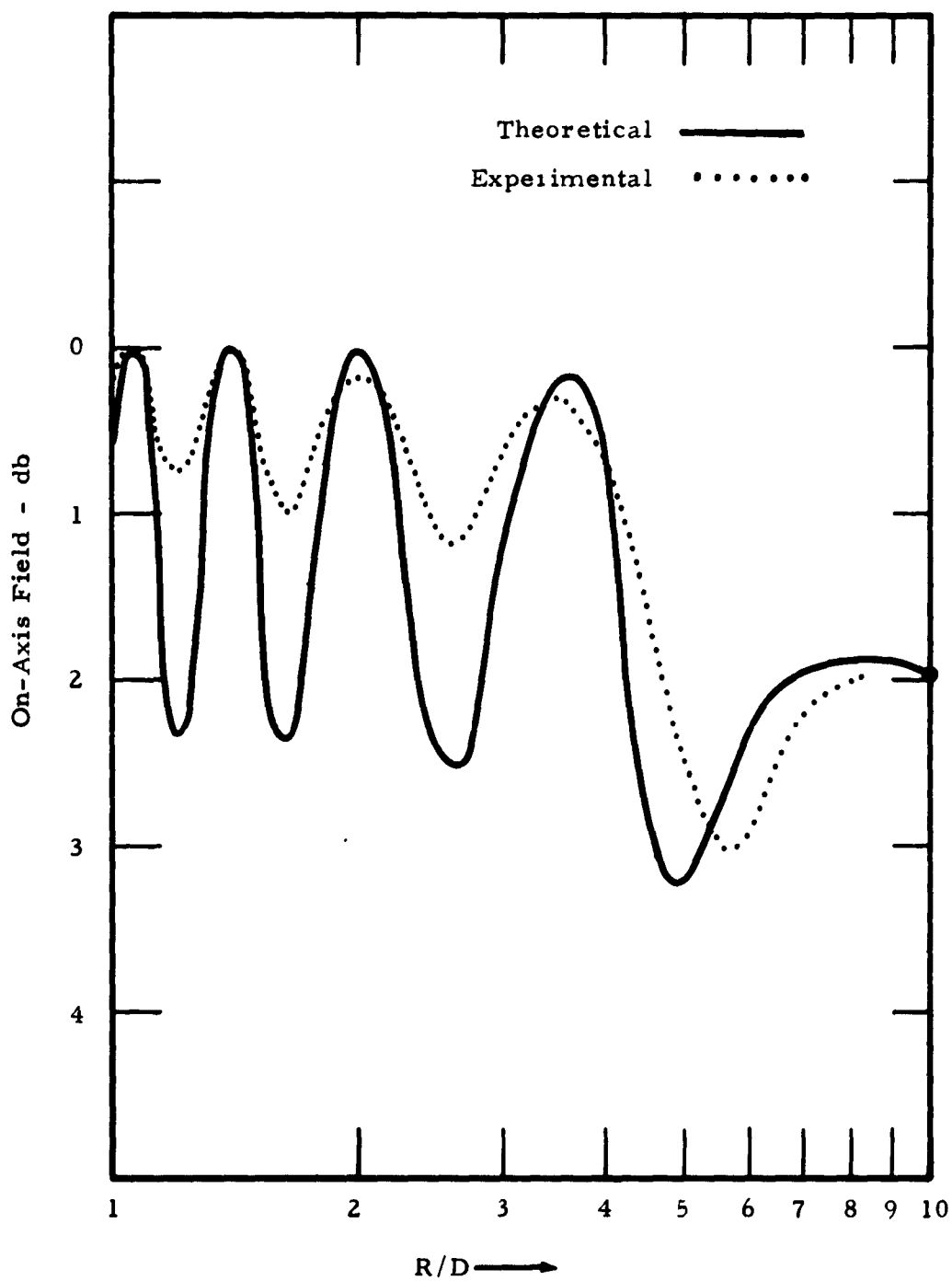


Figure 20. On-Axis Field of Four-Foot Paraboloid Reflector, -40λ Diameter at X-Band

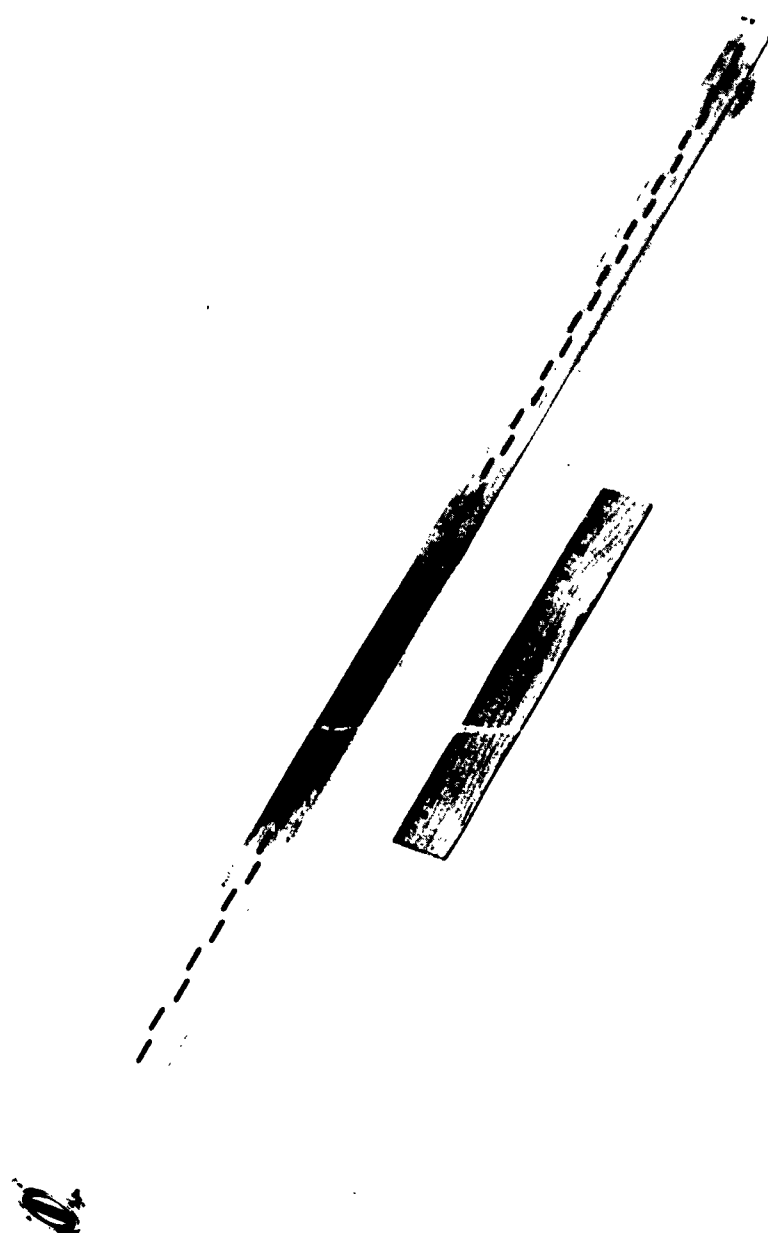


Figure 21. Forty-Element Linear Array

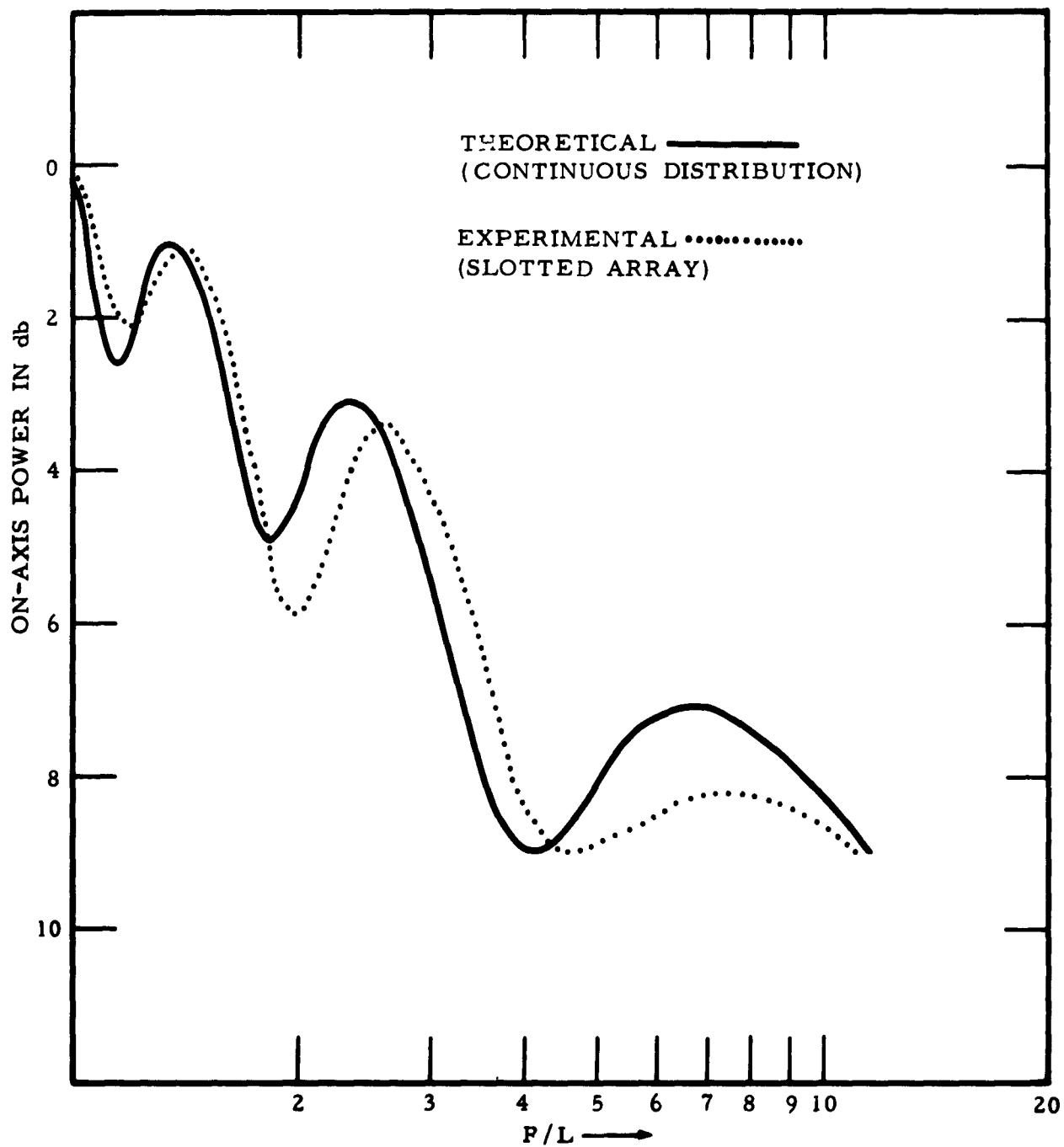


Figure 22. On-Axis Power — Uniformly Illuminated Line Source, $L = 27.3 \lambda$

4. Circular Planar Array

To complete the experimental work, measurements were made on a planar array made of five concentric rings of crossed slots cut in a standing-wave radial waveguide. A complete description of this array and the theory underlying its operation can be found in the literature.¹⁶ The array is pictured in Figures 23 and 24. The spacing between adjacent annuli is approximately one wavelength at the design frequency of 9375 Mc. Thus, the radial distribution cannot be approximated by a continuous distribution. However, it is seen that the spacing between crossed slots in a given annulus is quite small (approximately $\lambda/2$), and thus the azimuthal distribution can be taken to be continuous.

Establishing the E_{10} standing-wave mode in the radial waveguide results in a linearly-polarized aperture distribution, under the condition that the radial positions of the annuli correspond to the roots of the Bessel function $J_2(k\rho)$. Under this condition, the excitation of each annuli is proportional to $J_1(k\rho_n)/(k\rho_n)$. To obtain an in-phase distribution the annuli corresponding to odd values of n must be omitted. Under these conditions, and assuming the crossed slots to be infinitesimal and the azimuthal distribution to be continuous, the on-axis field is given by

$$F(R) = \sum_{n=1}^5 J_1(k\rho_{2n}) \frac{e^{-jk\sqrt{R^2 + \rho_{2n}^2}}}{\sqrt{R^2 + \rho_{2n}^2}} \quad (72)$$

The theoretical curve of on-axis field, as computed by Equation (72) is compared with the experimental curve in Figure 25. As in the case of the linear array, the agreement is seen to be very good, except for a slight discrepancy in the directions of the relative maxima and minima.

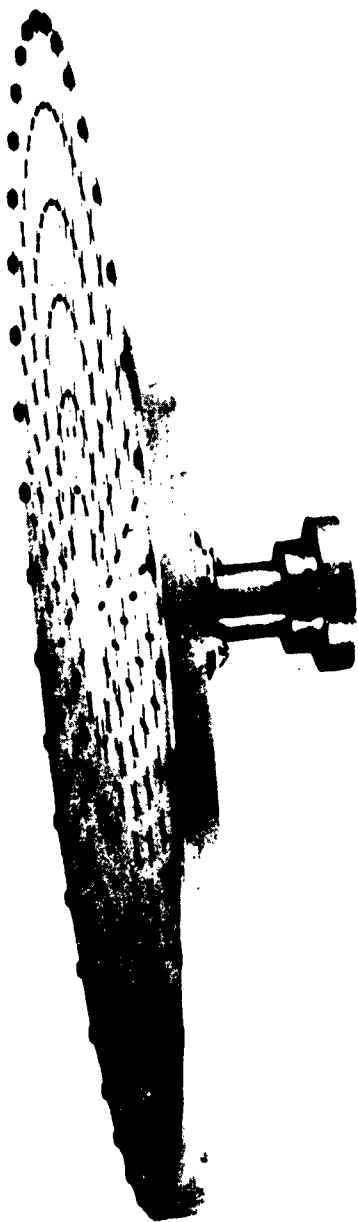
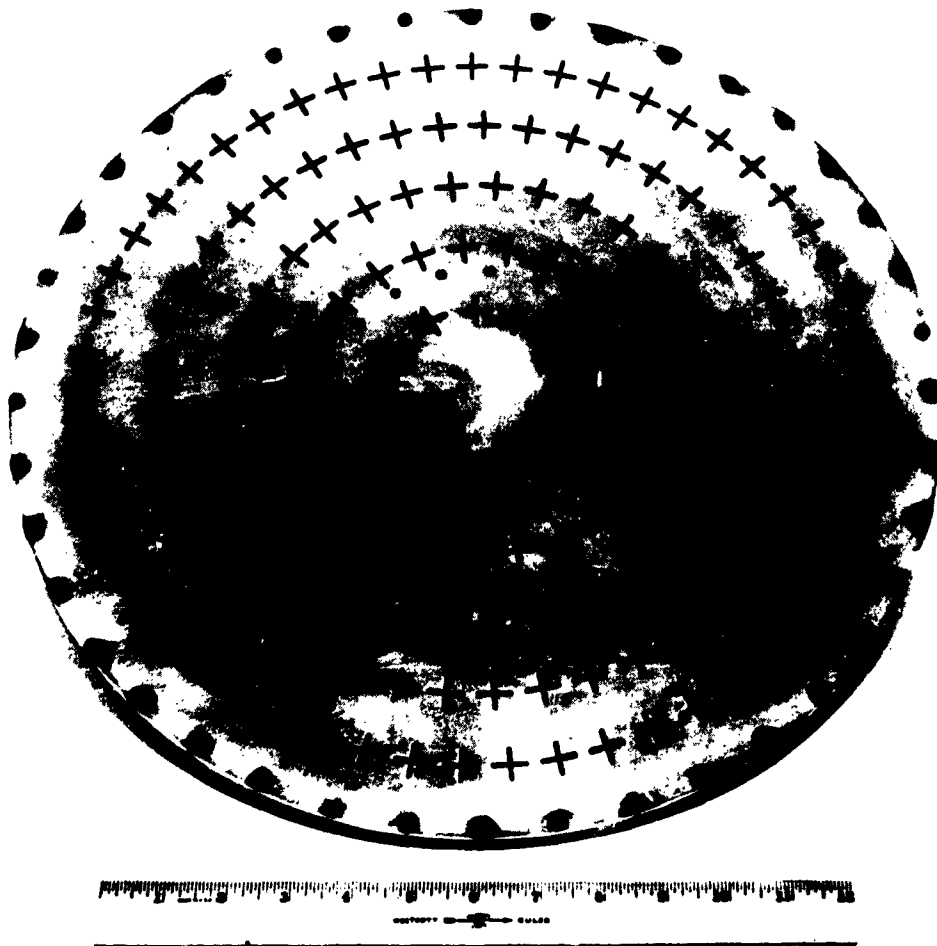


Figure 23. Circular Planar Array of Five Rings of Crossed Slots - Side View



**Figure 24. Circular Planar Array of Five Rings of Crossed Slots
- Front View**

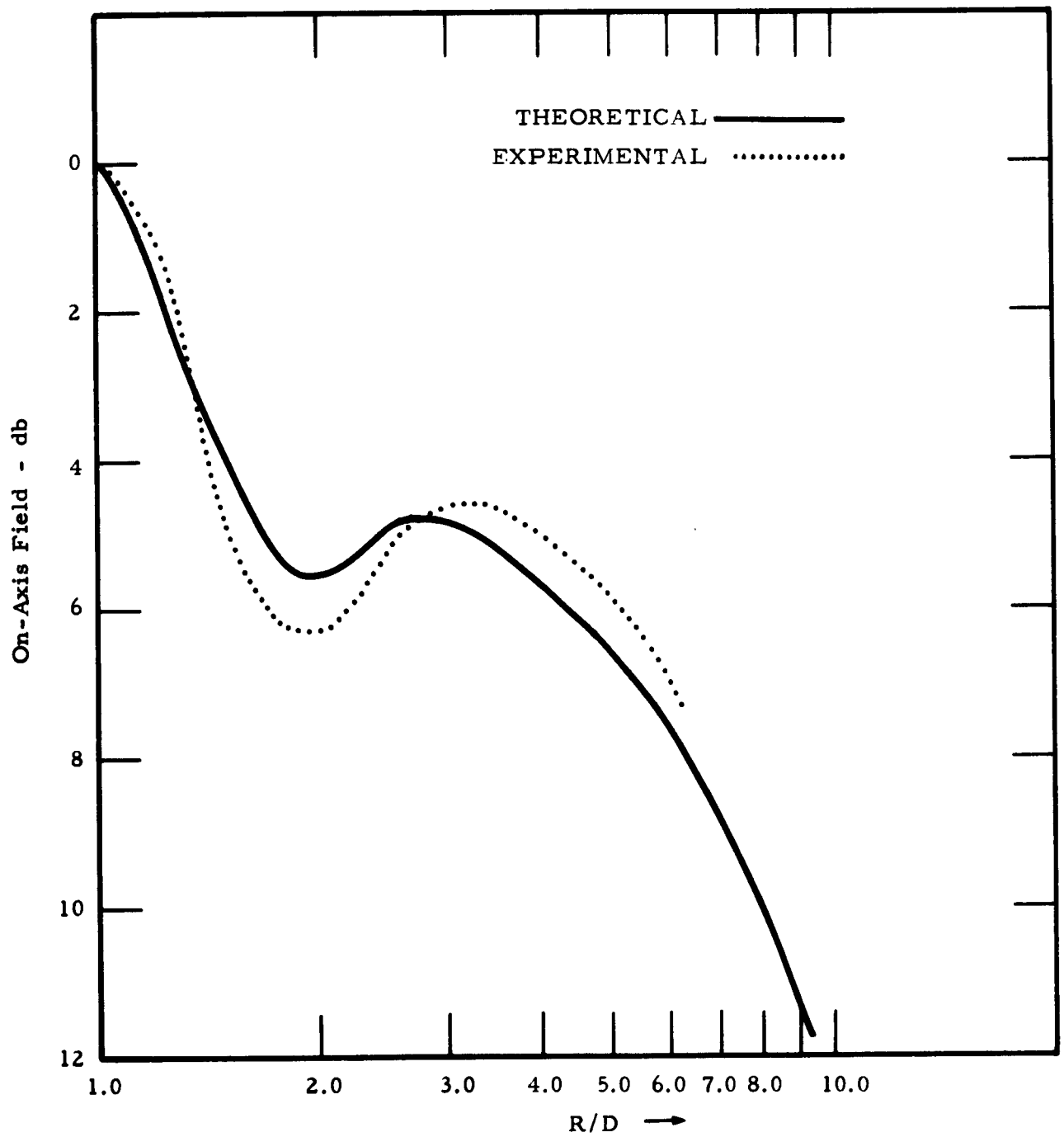


Figure 25. On-Axis Field for Circular Planar Array — Diameter is 10.73λ

IV. CONCLUSIONS

A number of conclusions can be drawn from the theoretical and experimental portions of the study. The transition distance analysis has shown that as the azimuthal angle increases the SNF tends towards the envelope of the far field pattern. Thus the transition distance is dependent upon the azimuthal angle as well as the aperture size, shape, and distribution. The first null transition distance, which is the longest, depends upon the sidelobe level and decay rate. The influence of the sidelobe level predominates. As the level decreases from -15 db to -40 db, the transition distance increases about fivefold. It varies from somewhat less than L^2/λ to $5L^2/\lambda$; the exact values depending upon the sidelobe taper. As the taper increases from zero to 8 db, the first null transition distance decreases by a factor of approximately one and one-half. The higher null transition distances are less dependent upon both sidelobe level and taper. In fact, for azimuthal angles that are large compared to the antenna's beamwidth, the transition distance approaches $L/\sin \theta$, regardless of the sidelobe level and taper.

Comparisons of the SNF of unequally sized apertures (both circular and rectangular) have demonstrated that universal patterns of the SNF can be constructed by considering a particular aperture size. This has allowed a set of field components from which one can construct the SNF of apertures that are arbitrary in both size and distribution, to be tabulated. The tables are presented in Volume II of this report. In the construction of the SNF, only simple multiplicative and additive operations are required. Thus, no specialized equipment is necessary although a desk-type calculator can be used to advantage.

The formulation was based upon aperture distributions of the form $1 + a_1 \rho^2 + a_2 \rho^4 + a_3 \rho^6$, which are capable of closely approximating most practical distributions. Similarities among the primary feed patterns of most high gain paraboloidal-type reflectors has allowed a universal set of aperture distribution parameters, a_n , to be determined as a function of the aperture taper. Thus estimates of the SNF of high-gain reflectors are easily obtained by the techniques developed. This is the case of most practical importance.

The experimental results described above indicate that the scalar near field formulation accurately describes the on-axis field of antennas to ranges as short as one diameter. This implies that the spatial impedance at that distance does not vary significantly from that of free space, and justifies calculating the power by simply squaring the field value.

The measurements made upon the 40λ paraboloidal antenna indicate that approximating the aperture distributions of reflecting-type antennas with functions of the form $1 + a_1 \rho^2 + a_2 \rho^4 + a_3 \rho^6$ allows accurate computations of the scalar near field. Further, the results indicate that the aperture distribution can be correctly deduced from primary feed pattern measurements.

Finally, the measurements on the array-type antennas show that the near field of antennas can be accurately calculated by a scalar formulation under the conditions that the aperture field is accurately known. Also, these results show that to within experimental error, the scalar near field of a continuous aperture is very similar to that of the corresponding discrete aperture.

V. RECOMMENDATIONS FOR FUTURE RESEARCH

Outlined below are several research areas which American Systems Incorporated feels should be pursued in connection with the study of the interference aspects of Fresnel region phenomena. Additionally, an approach to each study area is recommended.

A. Determination of the scalar near field (SNF) of elliptical apertures producing shaped beams in one plane: The SNF analysis must be extended to include the effect of the elliptical shape and the presence of a nonuniform phase distribution across the aperture which gives rise to diverging rays. Conceptually these factors present no great difficulty, since they merely modify the form of the scalar near field integral. By generalizing the results of the analyses discussed in Section III. C. 4 entitled, "Universal Patterns", it can be concluded that only one or two antenna sizes need be considered to obtain results which can be extrapolated to all sizes of interest. Thus this portion of the study can be adequately performed by theoretically investigating a limited number of special cases. It is felt that experimental verification should be obtained by performing measurements on at least one operational antenna of the Air Force's choosing.

B. Determination of the SNF of monopulse antennas: The SNF of monopulsed rectangular apertures can be obtained by a formulation identical to that derived in the present study, providing the aperture distribution function is appropriately modified. To obtain the SNF of circular apertures additional modification is necessary, however, since the aperture distribution function is no longer circularly symmetric. The modification is straightforward, however, requiring only minor modifications to the computer program. Thus, the scalar near field of monopulsed antennas, both

rectangular and circular, can be analyzed by straightforward extensions of the SNF formulation.

C. Spurious frequency response of antennas: The spurious frequency analysis initiated under the present contract should be extended to include a more detailed analysis of the frequency characteristics of the primary feed, and thus a more accurate description of spurious frequency aperture distribution. Where possible, experimental data on the harmonic distribution of energy should be used. Additionally, experimental work should be performed, and if possible on operational antennas.

D. Far field measurements in the near field: The single lens design described in Section III. F should be extended to a double lens design which will allow the amplitude variations to be undisturbed in the presence of the lens, while focusing the aperture at a finite range. The feasibility of this approach should be verified experimentally. Additionally, signal processing antenna ranges which permit far field measurement in the near field should be investigated.

E. Aperture field to scalar near field transition distance: A theoretical and experimental investigation which delineates the transition distance between the aperture field and the scalar near field is required to definitely establish the limits of validity of the scalar near field formulation. The theoretical investigation would proceed by investigating the differences in the field predicted by vector and scalar formulations, and by determining the radial components of field. Experimental work would allow a comparison of the measured field with that calculated by the scalar formulation and allow measurements of the radial components.

F. Electrically-scanned arrays: The effect on the SNF of a linear phase slope should be investigated by procedures similar to those used in the in-phase case.

G. Antenna-to-antenna coupling: A theoretical investigation of the near field coupling of energy between antennas should be pursued.

H. Terrain reflections: The problem of terrain reflections is best investigated by a modeling approach. One simple approach is to investigate the disturbance of the on-axis field by varying the antenna height above the ground.

I. Measurement Program: The results of the theoretical work should be verified by off-axis scalar near field pattern measurements in addition to the on-axis measurements made in compliance with the present contract.

APPENDIX I

ASYMPTOTIC REPRESENTATION OF THE TRANSITION DISTANCE

For a linear antenna whose aperture distribution is $J_0(iC\sqrt{\pi^2 - p^2})$ the transition distance can be written as

$$\frac{K\lambda R}{L^2} = \frac{\pi}{4} \frac{\gamma_{3/2,n}}{(\sin \gamma_{3/2,n})} \int_0^1 x^2 I_0(\pi C \sqrt{1-x^2}) \cos(\pi x \sqrt{n^2 + C^2}) dx \quad (I-1)$$

For n large, the following approximations are valid

$$\cos(\pi x \sqrt{n^2 + C^2}) \approx \cos\left(n\pi x + \frac{\pi C^2 x}{2n}\right) \approx \cos(n\pi x) - \frac{\pi C^2 x}{2n} \sin(n\pi x) \quad (I-2)$$

Using Equation (I-2), Equation (I-1) is divided into two integrals, each of which may be integrated repeatedly by parts, as follows

$$\begin{aligned} \int_0^1 x^2 I_0(\pi C \sqrt{1-x^2}) \cos(n\pi x) dx &= \left\{ x^2 I_0(\pi C \sqrt{1-x^2}) \frac{\sin(n\pi x)}{n\pi x} \right\} \Big|_0^1 \\ &+ \left\{ \frac{d}{dx} \left[x^2 I_0(\pi C \sqrt{1-x^2}) \right] \frac{\cos(n\pi x)}{(n\pi)^2} \right\} \Big|_0^1 \\ &+ \int_0^1 \frac{d^2}{dx^2} \left[x^2 I_0(\pi C \sqrt{1-x^2}) \right] \frac{\cos(n\pi x)}{(n\pi)^2} dx \quad (I-3) \end{aligned}$$

The first term on the right of Equation (I-3) vanishes by virtue of the limits and the contribution of the remaining integral is small for small n . Therefore,

$$\begin{aligned}
 \int_0^1 x^2 I_0(\pi C \sqrt{1-x^2}) \cos(n\pi x) dx &\sim \left\{ \frac{d}{dx} \left[x^2 I_0(\pi C \sqrt{1-x^2}) \right] \frac{\cos(n\pi x)}{(n\pi)^2} \right\} \Bigg|_0^1 \\
 &= \left\{ \left[2x I_0(\pi C \sqrt{1-x^2}) + x^2 \pi C \frac{-2x}{2\sqrt{1-x^2}} I_1(\pi C \sqrt{1-x^2}) \right] \frac{\cos(n\pi x)}{(n\pi)^2} \right\} \Bigg|_0^1 \\
 &= \left[2 - \pi C \lim_{x \rightarrow 1} \frac{I_1(\pi C \sqrt{1-x^2})}{\sqrt{1-x^2}} \right] \frac{(-)^n}{(n\pi)^2} \\
 &= (-)^n \frac{2 - \frac{1}{2} (\pi C)^2}{(n\pi)^2} \tag{I-4}
 \end{aligned}$$

Similarly,

$$- \frac{\pi C^2}{2n\pi} \int_0^1 x^3 I_0(\pi C \sqrt{1-x^2}) \sin(n\pi x) dx \sim (-)^n \frac{(\pi C)^2}{2(n\pi)^2} \tag{I-5}$$

From Equations (I-4) and (I-5) the transition distance becomes

$$\frac{K\lambda R}{L^2} \sim (-)^n \frac{1}{2n^2 \pi} \frac{\gamma_{3/2,n}}{(\sin \gamma_{3/2,n})}$$

But $\gamma_{3/2,n}$ is the n^{th} root of $J_{3/2}(x)$ and for n large, $\gamma_{3/2,n} = \frac{2n+1}{2} \pi$;
also, $\sin (\gamma_{3/2,n}) = (-)^n$, therefore

$$\frac{K\lambda R}{L^2} \sim \frac{2n+1}{4n^2} \tag{I-6}$$

which is the desired answer.

APPENDIX II

PROGRAM FOR THE EVALUATION OF $J_\nu(x)$

To numerically evaluate $J_\nu(x)$ for large values of ν , the $x - \nu$ plane has been divided into seven regions as shown in Figure 26. In region (a), the phase amplitude method of Goldstein and Thaler¹⁹ has been used. This has allowed the numerical evaluation of the Bessel functions for orders of 50 and less, and for arguments of 50 or less.

In region (b), in which $\nu > 50$ and $x/\nu \leq 1.5$, asymptotic formulations valid for large orders and arguments have been used to evaluate $J_\nu(x)$. The equations used are Equations (3), (5), and (6) of article 4.35.1, page 87 of Reference 20. In region (c), values were obtained by recursing forward (i.e., increasing ν) from region (b). The forward recursion was accomplished with facility to values of $x/\nu \geq 1.2$. For $x/\nu \leq 1.2$, the Bessel function becomes small (although not negligible) and the forward recursion technique loses accuracy. To overcome this difficulty a formulation valid in the immediate vicinity of $x = \nu$ was used to determine $J_\nu(x)$ in the narrow strip $\nu - 1 \leq x \leq \nu + 1$. This formulation is given by Equations (1), (3), (4), and (5) of article 4.34.2, pages 87 through 88 of Reference 20. Using the values thus obtained, values in region (d) were obtained by backward recursion, and values in region (e) by forward recursion. With a knowledge of the correct values in region (e), the ratio method was used to determine the values in region (f).^{21,22} This method involves assuming a value in a region in which the Bessel function is not known [region (g)], applying the recursion formulas backward to a region in which the correct answer is known, and comparing the obtained results with the known value. In region (g), $J_\nu(x) < 10^{-10}$ and is neglected.

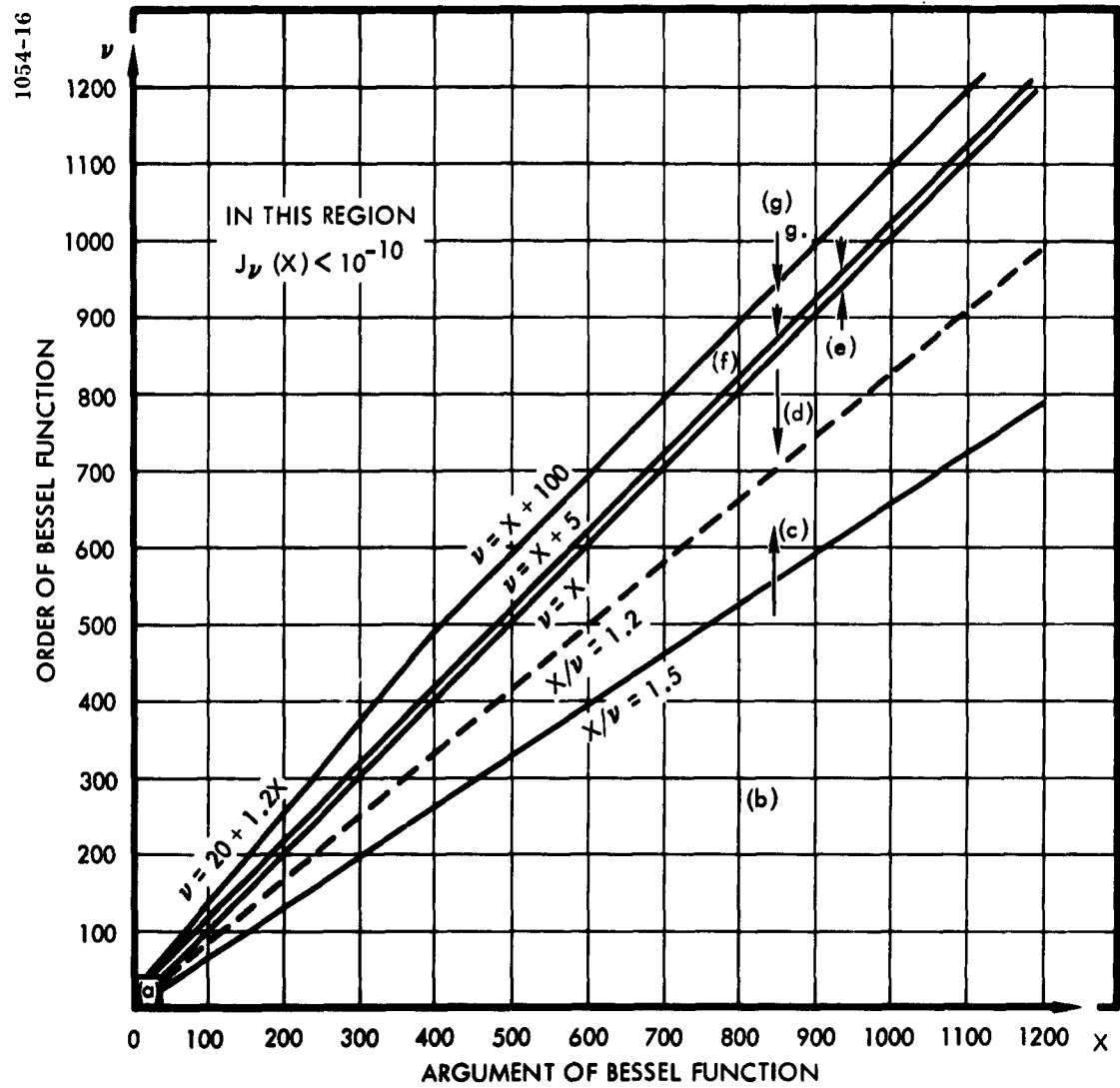


Figure 26. Division of ν - x Plane

REFERENCES

1. S. Silver. Microwave Antenna Theory and Design, McGraw-Hill Book Company, Inc., New York, New York (1949), pp. 170-174.
2. C. Polk. "Optical Fresnel-Zone Gain of a Rectangular Aperture", IRE Transactions on Antennas and Propagation, vol. AP-4 (January 1956), pp. 65-69.
3. R. W. Bickmore and R. C. Hansen. "Antenna Power Densities in the Fresnel Region", Proceedings of the IRE, vol. AP-4 (December 1959).
4. R. C. Hansen and L. L. Bailin. "Near Field Analysis of Circular Aperture Antennas", Scientific Report No. 3508/3, Contract AF 19(604)-3508, August 1959, Hughes Aircraft Company.
5. R. W. Bickmore and R. J. Spellmire. "A Two-Parameter Family of Line Sources", Technical Memo No. 595, October 1956, Hughes Aircraft Company.
6. T. T. Taylor. "Design of Circular Apertures for Narrow Beamwidth and Low Sidelobes", IRE Transactions on Antennas and Propagation, vol. AP-3 (January 1955), pp. 16-28.
7. T. T. Taylor. "Design of Circular Apertures for Narrow Beamwidth and Low Sidelobes", IRE Transactions on Antennas and Propagation, vol. AP-8 (January 1960), pp. 17-22.
8. T. T. Taylor. "One Parameter Family of Line Sources Producing Modified $\sin \pi u / \pi u$ Patterns", Technical Memo No. 324, September 1953, Hughes Aircraft Company.
9. H. Jasik. Antenna Engineering Handbook, McGraw Hill Book Co., Inc., New York, New York (1961), pp. 12-4 to 12-8.
10. W. D. Hayes. "Gratings and Screens as Microwave Reflectors", Report 54-20, 1 April 1943, Radiation Laboratory.
11. A. C. Wilson and H. V. Cottony. "Radiation Patterns of Finite-Size Corner-Reflector Antennas", IRE Transactions on Antennas and Propagation, vol. AP-8 (March 1960), pp. 144-157.

REFERENCES (Continued)

12. W. E. Groves. "Transmission of Electromagnetic Waves Through Pairs of Parallel Wire Grids", Doctoral Thesis in Electrical Engineering, 4 September 1951, University of California.
13. W. W. Mumford. "Some Technical Aspects of Microwave Radiation Hazards", Proceedings of the IRE, vol. 49 (February 1961), pp. 427-447.
14. R. W. Bickmore. "Fraunhofer Pattern Measurement in the Fresnel Field", Scientific Report No. 8, Contract AF 19(604)-1317, Hughes Aircraft Company.
15. H. H. Hougardy. "Study and Design of a Time/Frequency Near Zone Pattern Range", Technical Report No. 61-ESD-1, 28 April 1961, American Systems Incorporated.
16. H. H. Hougardy. "Transverse Doppler Pattern Measurement Technique", Technical Report No. 62-ESD-9, Contract AF 19(604)-8362, 28 February 1962, American Systems Incorporated.
17. K. S. Kelleher. "Antenna Wavefront Problems", Report No. 3530, September 1949, Naval Research Laboratories.
18. F. J. Goebels and K. C. Kelly. "Arbitrary Polarization from Annular Slot Planar Arrays", IRE Transactions on Antennas and Propagation, vol. AP-9 (July 1961), pp. 342-349.
19. M. Goldstein and R. M. Thaler. "Bessel Functions for Large Arguments", Mathematical Tables and Other Aids to Computation, vol. XII, No. 61 (January 1958).
20. N. W. McLachlan. Bessel Functions for Engineers, Oxford University Press, London, E. C. 4 (1955), p. 87.
21. M. Goldstein and R. M. Thaler. "Recurrence Techniques for the Computation of Bessel Functions", Mathematical Tables and Other Aids to Computation, vol. XIII, No. 66 (April 1959).
22. F. J. Carbato. "Generation of Spherical Bessel Functions in Digital Computers", vol. VI, No. 3, July 1959.

GENERAL BIBLIOGRAPHY

In addition to the papers referenced in the previous sections, considerable work has been carried on in this field. The following is a general bibliography indicating the extent of this activity. It was used as background material in the performance of the study program.

R. A. Gerlock. "Study of Interference Aspects of Fresnel Region Phenomenon", 61-ESD-2, First Quarterly Memorandum, Contract AF 30(602)-2507, 29 August 1961, American Systems Incorporated.

R. A. Gerlock. "Study of Interference Aspects of Fresnel Region Phenomenon", 61-ESD-6, Second Quarterly Memorandum, Contract AF 30(602)-2507, 1 November 1961, American Systems Incorporated.

R. A. Gerlock. "Study of Interference Aspects of Fresnel Region Phenomenon", 62-ESD-10, Third Quarterly Memorandum, Contract AF 30(602)-2507, 3 February 1962, American Systems Incorporated.

R. B. Barrar and A. F. Kay. "A Series Development of a Solution of the Wave Equation in Powers of $1/r$ ", Paper presented at the URSI Meeting in Washington, D. C. , May 1954.

R. B. Barrar and C. H. Wilcox. "The Fresnel Field of a Finite Line Current Distribution", Scientific Report No. 4, Contract AF 19(604)-1317, February 1955, Hughes Aircraft Company, Culver City, California.

R. B. Barrar and C. H. Wilcox. "On the Fresnel Approximation", IRE Transactions on Antennas and Propagation, vol. AP-6 (January 1958), pp. 43-48.

Bates and Elliott. "The Determination of the True Sidelobe Level of Long Broadside Arrays from Radiation Pattern Measurements Made in the Fresnel Region", Proceedings of the IEE, Part c (September 1956).

R. W. Bickmore. "On Focusing Electromagnetic Radiators", Canadian Journal of Physics, vol. 35 (November 1957), pp. 1292-1298.

General Bibliography (continued)

- R. W. Bickmore. "Fraunhofer Pattern Measurement in the Fresnel Region", Canadian Journal of Physics, vol. 35 (November 1957), pp. 1299-1308.
- R. W. Bickmore. "A Focusing Criterion for Rectangular Apertures", Technical Memo No. 376, Hughes Aircraft Company.
- R. W. Bickmore. "On the Transmission between Two Rectangular Apertures", Scientific Report No. 1, Contract AF19(604)-1317, March 1955, Hughes Aircraft Company.
- R. W. Bickmore. "Power Transmission via Radio Waves", Proceedings of the IRE, vol. 48, No. 3, March 1960.
- R. W. Bickmore. "A Note on the Effective Aperture of Electrically Scanned Arrays", IRE Transactions on Antennas and Propagation, vol. AP-6 (April 1958), pp. 194-196.
- R. W. Bickmore and R. C. Hansen. "Antenna Power Densities in the Fresnel Region", Proceedings of the IRE, vol. 47, No. 12 (December 1959), pp. 2119-2120.
- C. J. Bouwkamp. "Diffraction Theory", Reports on Progress in Physics, vol. 12 (1954).
- E. H. Braun. "Gain of Electromagnetic Horns", Proceedings of the IRE, vol. 41 (January 1953), pp. 109-115.
- D. K. Cheng. "On the Simulation of Fraunhofer Radiation Patterns in the Fresnel Region", Transactions of the IRE, vol. AP-5 (October 1957), pp. 399-402.
- A. L. Cullen. "A General Method for the Absolute Measurement of Microwave Power", IEE Monolog No. 23 (15 February 1952). Also in Proceedings of the IEE, pt. IV, vol. 99 (April 1952), pp. 112-120.
- R. L. Dondero. "Determination of Power Densities at Microwave Frequencies", Proceedings of the First Annual Tri-Service Conference on Biological Hazards of Microwave Radiation (at RADC, Griffiss Air Force Base, New York), Appendix F (15-16 July 1957), pp. 115-118.

General Bibliography (continued)

R. F. Goodrich and R. E. Hiatt. "On Near Zone Antennas", Final Report 2861-1-F for General Electric, June 1959, University of Michigan.

M. Handelsman. "Technical Note on Focusing Properties of a Linear Antenna with a Spherical Phase Front", DCS/Operations, RADC, Griffiss Air Force Base, New York (October 1958).

R. C. Hansen and L. L. Bailin. "Near Field Analysis of Circular Aperture Antennas", Scientific Report No. 3, Contract AF19(604)-3508, August 1959, Hughes Aircraft Company.

R. C. Hansen and L. L. Bailin. "A New Method of Near Field Analysis", IRE Transactions on Antennas and Propagation, vol. AP-7 (1959 special issue on Toronto Symposium).

R. C. Hansen, L. L. Bailin, and R. W. Rutishauser. "On Computing Radiation Integrals", Comm. Assoc. Computing Machinery, vol. 2 (February 1959), pp. 28-31.

R. F. Harrington, A. T. Villeneuve, and M. K. Hu. No Title, Antenna Research Reports No. EE619-5812P1 (December 1958), EE619-593P2 (March 1959), and EE619-597F (September 1959), on General Electric subcontract, Syracuse University.

E. Jacobs. "Fresnel Region Patterns and Gain Corrections of Large Rectangular Antennas", Fifth Conference on Radio Interference Reduction and Electronic Capability, Chicago, 1959.

E. Jacobs. "Predicting the Antenna's Role in RFI", Electronic Industries, vol. 19, No. 5 (May 1960), pp. 96-102.

E. Jacobs and O. M. Sakati. "The Gain of Aperture Antennas at Spurious Frequencies", Fifth Conference on Radio Interference Reduction and Electronic Compatibility, Chicago, 1959.

R. Justice and V. H. Rumsey. "Measurement of Electric Field Distribution", IRE Transactions on Antennas and Propagation, vol. AP-3 (October 1955), pp. 177-180.

General Bibliography (continued)

A. L. Haywood. "The Mathematics of Fresnel Region Field Distribution for Plane Rectangular Aperture Antennas", WADC-TR-59-462, August 1959, Aerial Reconnaissance Laboratory, Wright Air Development Center.

A. L. Haywood. "Radar Radiation Hazards in the Near Field of Aperture Antennas", WADD-TR-60-551, October 1960, Reconnaissance Laboratory, WADD.

O. E. Horton. "Measurements of Radar Power Density Levels to Establish Nonhazardous Working Area", Memo No. WCLRS-6-58-4, March 1958, Wright Air Development Center.

M. K. Hu. "Study of Near-Zone Fields of Large Aperture Antennas", Final Report No. RADC-TR-57-126A and B, April 1957, Syracuse University.

M. K. Hu. "Some New Methods of Analysis and Synthesis of Near Zone Fields", 1960 IRE Convention Record, Part 1 (March 1960).

M. K. Hu. "On Measurements of Microwave E- and H-Field Distributions Using Modulated Scattering Methods", IRE Transactions in Microwave Theory and Techniques, vol. MTT-8, No. 3 (May 1960).

M. K. Hu. "Antenna Research: Part III - Synthesis Methods of Fresnel Region and Near Zone Fields", Technical Report No. 2, March 1959, Syracuse University Research Institute.

A. F. Kay. "Near Field Gain of Aperture Antennas", IRE Transactions on Antennas and Propagation, vol. AP-8 (November 1960).

A. F. Kay. "Far Field Data at Close Distances", Contract AF19(604)-1126, October 1956, Technical Research Group, Inc., New York.

A. F. Kay. "Near Field Gain", Report No. SR 131-1, Contract AF19(604)-5532, August 1959.

K. C. Kelly. "Angle Deception Radar Reflections", Technical Memo No. 594, August 1959, Hughes Aircraft Company, Microwave Lab.

General Bibliography (continued)

Tsu Kennaugh. "Multipole Field Expansions and Their Use in Approximate Solutions of EM Scattering Problems", Report No. 827-5, November 1959, Ohio State University.

Tsu Kennaugh. "Approximate Solutions to Scattering Problems by Multipole Matching", Report No. 827-4, July 1959, Ohio State University.

Little. "Gain Measurements of Large Aerials Used in Interferometer and Cross-Type Radio Telescopes", Australian Journal of Physics, (1958), pp. 70-78.

E. Lommel. "Theoretical and Experimental Investigations of Diffraction Phenomena at a Circular Aperture and Obstacle", Bayerisch, Okad, and Wiss, vol. 15 (1884), pp. 233 (translated by G. Bekefi and G. A. Wooton, McGill University).

W. W. Mumford. "Some Technical Aspects of Microwave Radiation Hazards", Proceedings of the IRE, vol. 49, No. 2 (February 1961).

Polk. "Optical Fresnel-Zone Gain of a Rectangular Aperture", IRE Transactions on Antennas and Propagation, vol. AP-4 (January 1956), pp. 65-69.

Polk. "Discussion of Some Terms Used in Describing Radiation from Small and Large Antennas", Unpublished Technical Memo No. 5410-19, Contract AF30(602)-583, August 1956, Hughes Aircraft Company.

J. H. Richmond. "A Modulated Scattering Technique for Measurement of Field Distributions", IRE Transactions on Microwave Theory and Techniques, vol. MTT-3 (July 1955), pp. 13-15.

J. Robieux. "Near-Zone Power Transmission Formulas", Proceedings of the IRE, vol. 47 (June 1959), pp. 1161-1163.

V. Rumsey. "Reaction Concept in Electromagnetic Theory", Physics Review, vol. 94 (June 1954), pp. 1483-1491.

W. G. Sterns. "Near-Zone Field Studies of Quasi-Optical Antennas", Thesis, circa 1954, University of California at Berkeley.

General Bibliography (continued)

B. J. Strait. "Microwave Diffraction Field Measurements by Modulated Scattering Techniques", Report No. EE492-6005T9, May 1960, Syracuse University Research Institute (Task Report No. 9, RADC-TN-60-115).

M. Sucher. "A Comparison of Microwave Power Measurement Techniques", Proceedings of Symposium on Modern Advanced in Microwave Techniques, Polytechnic Institute of Brooklyn, 8-10 November 1954, pp. 309-323.

G. Swarup and K. S. Yang. "Monitoring Paraboloidal Antennas", Proceedings of the IRE, vol. 48 (November 1951), pp. 1918-1919.

S. Tetelbaum. "On Some Problems of the Theory of Highly Directive Antenna Arrays", Journal of Physics (U. S. S. R.), vol. 10, No. 3 (1946), p. 285.

A. T. Villeneuve. "Antenna Research, Part VI - Near Zone Pattern Synthesis by the Focusing Method", Final Report, September 1959, Syracuse University Research Institute.

M. I. Willinski. "Beamed Electromagnetic Power as a Propulsion Energy Source", Journal of American Rocket Society, vol. 29 (August 1959), pp. 601-603.

"Industrial Hazards", RADC Regulation NR 160-1, RADC, Griffiss Air Force Base, New York, 31 May 1957.

"Microwave Radiation Hazards", Urgent Action Technical Order 31-1-511, Rome Air Force Depot, Griffiss Air Force Base, 17 June 1957.

"Radio Frequency Hazards", Handbook BuAer or USAF Technical Order 31-1-80, 15 April 1958.

"Radio Frequency Radiation Hazards", Handbook BuAer or USAF Technical Order 31-1-80, 15 April 1958 (Revised 15 May 1958).

"Raytheon Microwave Powered Helicopter", Time, vol. 73, 25 May 1959, p. 55.

General Bibliography (continued)

"Air Force Radio Frequency Radiation Hazards Handbook", USAF Technical Order 31P-1-15, Rome Air Force Depot, Griffiss Air Force Base, 1 November 1954.